BRL

REPORT NO. 1659

EVALUATION OF THE COMPUTER CODES BLAST, DORF, HELP AND HEMP FOR SUITABILITY OF UNDEREXPANDED JET FLOW CALCULATION

by

Csaba K. Zoltani

August 1973

USA BALLISTIC RESEARCH LABORATORIES
ABERDEEN PROVING GROUND, MARYLAND

Destroy this report when it is no longer needed.
Do not return it to the originator.

Secondary distribution of this report by originating or sponsoring activity is prohibited.

Additional copies of this report may be obtained from the National Technical Information Service, U.S. Department of Commerce, Springfield, Virginia 22151.

The findings in this report are not to be construed as an official Department of the Army position, unless so designated by other authorized documents.

B A L L I S T I C R E S E A R C H L A B O R A T O R I E S

BRL REPORT NO. 1659

AUGUST 1973

EVALUATION OF THE COMPUTER CODES BLAST, DORF, HELP AND HEMP FOR SUITABILITY OF UNDEREXPANDED JET FLOW CALCULATION

Csaba K. Zoltani
Applied Mathematics Laboratory

RDT&E Project No. 1J562604A607

A B E R D E E N P R O V I N G G R O U N D, M A R Y L A N D

INTENTIONALLY LEFT BLANK.

B A L L I S T I C R E S E A R C H L A B O R A T O R I E S

BRL Report No. 1659

CKZoltani/cas
Aberdeen Proving Ground, MD.
August 1973

EVALUATION OF THE COMPUTER CODES BLAST, DORF HELP AND HEMP FOR SUITABILITY OF UNDEREXPANDED JET FLOW CALCULATION.

ABSTRACT

The computer codes BLAST, DORF, HELP and HEMP have been used to simulate the flow field at the muzzle of a M-16 rifle, without any deflectors, compensators, or flash hiders. The flow was modeled as an underexpanded jet, of a compressible, inviscid and non-reactive gas. The calculations, restricted to the initial stages of formation of the jet were done on a cylindrically symmetric geometry without the presence of a flow obstruction in the form of a projectile. Results are presented as pressure contours as well as pressure and velocity profiles at different angles from the centerline of the muzzle of the barrel, and plots of pressure versus distance from the muzzle. The calculations have been compared with available photographic records of the process.

INTENTIONALLY LEFT BLANK.

TABLE OF CONTENTS

INTENTIONALLY LEFT BLANK.

LIST OF ILLUSTRATIONS

LIST OF SYMBOLS

A	material constant
a	material constant
B	material constant
b	material constant
C	velocity of sound
D	nozzle exit diameter
f	vector
h	mesh dimension
E	specific energy
I	specific internal energy
M	mass
M_x	Mach number
n	normal vector
P	pressure
q	artificial viscosity
r	radial distance
S	deviatoric stress increment surface in equations (16)-(18)
s	surface element
t	time
u	velocity in the x (or r) direction
V	cell volume
w	vector
X	distance from nozzle exit to first Mach disk
x	co-ordinate
Y_o	yield strength of material
z	axial distance

Greek Symbols

α	a function of the stress component
β	co-volume
γ	ratio of specific heats
ϵ	increment in deviatoric strain

η ρ/ρ_o

μ $\eta-1$

ρ density

Σ stress

σ Courant number

Subscripts

a area

i co-ordinate

L cell to the left of the one under investigation

k designates a cell

m co-ordinate

o initial value

R cell to the right of the one under investigation

T total

XX
XY
YY first index gives the axis to which the surface element, on which the stress is acting is perpendicular, and the second index the direction of the stress

1 refers to quadrilateral 1 in figure 4.

∞ ambient condition

Superscripts

1 defined by equation 11

n time level

~ intermediate value

I. INTRODUCTION

Improved accuracy of fire is the overriding concern of evolving weapons technology. In this quest, the designer is greatly aided by the availability of combustion gases which can compensate for launch errors. Muzzle devices, by properly channeling these gases, accomplish this task.

An extensive survey of the literature[1], however, revealed that no theoretical analysis exists which could serve as a basis for the design of these devices. Indeed, no gas flow model, able to predict the flow parameters with any degree of accuracy, has appeared.

Recent attempts at predicting the flow field at the muzzle of a gun have only met with partial success. Aside from the calculation of overpressure at some distance from the gun, such as those of references 2 through 5, the codes employed have been unable to give flow details needed for rational design improvements. Indeed, some of the results do not compare favorably with experimental results. Examples are the wrong flow shape in reference 6, the wrong Mach disk location in ref. 7, or even the failure of the widely used RIPPLE code to work beyond a few microseconds of real time.[8]

In the light of this assessment it was felt that, as a first step toward establishing our muzzle blast calculational capability and before embarking on a new code development, the most promising codes available at BRL should be tried to ascertain whether they could "simulate" the flow in fine enough detail at the muzzle of a M-16 rifle. The codes chosen were BLAST[6], DORF[9], HELP[10], and HEMP[11]*. This report summarizes the undertaking.

The report is organized as follows: in chapter two the flow model and the initial conditions are discussed. This is followed by a description of the salient features of the computer codes in chapter three. The calculational results, including the criteria for evaluation is given next. We summarize our conclusion in the last chapter.

II. DESCRIPTION OF THE FLOW TO BE SIMULATED

A. The Flow Model

The dynamics of the development of the flow is illustrated in Figure 1. In particular, as the projectile starts to move down the gun tube, it pushes a column of air ahead of it. This compressed air exits the tube pushing ahead of it a spherical, weak precursor shock. In the mean time, while the projectile is still in the tube, the hot, high pressure gases leak around it and escape from the tube.

As the projectile emerges from the tube it has to traverse and interact with the cloud of burnt gases. At this stage the propellant gases actually move faster than the projectile. Consequently, in addition to a precursor shock ahead of the projectile and the Mach disk formed by the exhaust gases at a few calibers from the tube, we also have a backward facing shock at the base of it. At a distance of ten to fifteen calibers from the gun tube, the picture changes, the bullet having acquired sufficient kinetic energy to enable it to outrun the propellant gas, punches through the precursor shock and enters the free flight stage. At this point our interest in the gas flow ceases.

In the presence of muzzle attachments, such as compensators or flash hiders, the flow is much more complicated with the flow interacting with the flow obstruction resulting in the reflection of shock waves and rarefactions. The present study doesn't consider the effects of such devices. Rather we model the development of the flow at and near the muzzle at early times, that is, within the first few microseconds of the process.

The pressure inside the tube is much higher than the ambient pressure. As the gases exhaust through the muzzle, the jet expands to the ambient pressure increasing its cross sectional area and creating the "shock bottle" configuration of an underexpanded jet. This comes about as follows: as the expansion waves from the lip of the nozzle reach the constant pressure boundary of the jet, they are reflected as compression waves and coalesce to form a shock. For slightly underexpanded nozzles, the intercepting shocks meet at the flow axis leading to the diamond configuration. For great pressure ratios, however, the shocks are connected by a Mach disk. Past the Mach disk the flow is subsonic bounded above by the slipstream originating from the triple point.

B. The Equations of Motion and Boundary Conditions

The flow simulation was done on an axisymmetric geometry as shown in figure 2. We assume that there are no muzzle attachments and no flow obstruction, in the form of a projectile, is present. The state of the high pressure gases was taken to be equivalent to that of the combustion gases generated in the firing of a M-16 rifle with a 1.795×10^{-3}kg charge. Since we were only trying to simulate the first few microseconds of the history of the flow, the tube containing the high pressure gases was allowed to empty and no attempts were made to impose either choking or real time dependent conditions at the muzzle. The surrounding were taken to be standard atmosphere at rest while the combustion products were taken to be a gas, without particulate matter, with a $\gamma=1.24$ at the conditions given later in this section.

a.

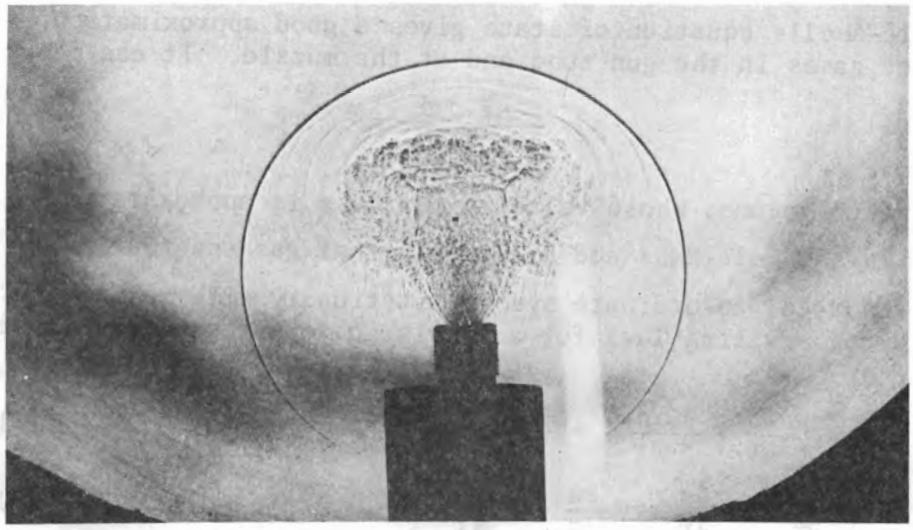

b.

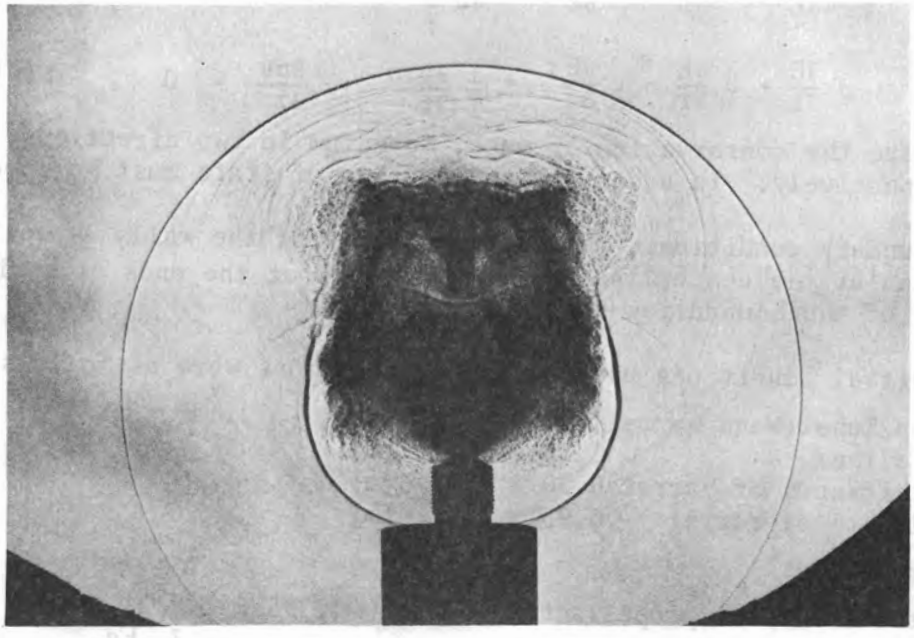

Figure 1 Stages of Muzzle Blast Development.

a. The Jet Formed by the Blowby Gases with the Projectile still in the Gun Barrel. Note the Mach Disc and the Triple Shocks Surrounded by a Region of Intense Turbulence.

b. Generation of the Secondary Blast Due to the Explosion of the Unburnt Propellant Gases. An Interesting Feature of the Flow Field is the "Bow Shock" on the Base of the Projectile.

Shadowgraphs Courtesy of Mr. D. Shear, EBL of BRL, M-16 Projectile from Mann Barrel. Velocity of Projectile 970 m/s.

The Noble-Abel's equation of state gives a good approximation to the product gases in the gun tube and at the muzzle. It can be written as

$$p = \frac{RT}{\frac{1}{\rho} - \beta} \frac{1}{M_i} \qquad (1)$$

where β is the co-volume, whose value in our case is approximately $1.0 cm^3/g$, M_i is the mole mass and R the universal gas constant.

In a cylindrical co-ordinate system, stationary with respect to the gun tube, the conservation laws for an inviscid, compressed gas are the following:

$$\frac{\partial \rho}{\partial t} + \frac{\partial (r\rho u)}{\partial r} + \frac{\partial (\rho v)}{\partial z} = 0 \qquad (2)$$

$$\rho \frac{\partial u}{\partial t} + u \frac{\partial u}{\partial r} + v \frac{\partial u}{\partial z} + \frac{\partial p}{\partial r} = 0 \qquad (3)$$

$$\rho \frac{\partial v}{\partial t} + u \frac{\partial v}{\partial r} + v \frac{\partial v}{\partial z} + \frac{\partial p}{\partial z} = 0 \qquad (4)$$

$$\rho \frac{\partial E}{\partial t} + u \frac{\partial E}{\partial r} + v \frac{\partial E}{\partial z} + \frac{1}{r} \frac{\partial pru}{\partial r} + \frac{\partial pv}{\partial z} = 0 \qquad (5)$$

These are the conservation of mass, momentum in two directions, and energy, respectively. In addition, an equation of state must be specified.

For boundary conditions, the impermeability of the walls as well as reflection at the centerline and free outflow at the ends or a rigid wall at one of the boundaries were specified.

The initial conditions used in the calculations were as follows:

1. Gun Tube (Mann barrel)

caliber	5.56×10^{-3}	[m]
thickness of barrel	0.50×10^{-2}	[m]
length of barrel	6.93×10^{-1}	[m]

2. Propellant

total mass of propellant	1.795×10^{-3} [kg]
propellant density	1.605×10^{3} $[\frac{kg}{m^3}]$
flame temperature	3.360×10^{3} [°K]
explosive force (zero deterrent)	1.115×10^{5} [m]
mole mass	2.56×10^{-2} $[\frac{kg}{mol}]$
co-volume	1.174×10^{-3} $[\frac{m^3}{kg}]$

3. Ambient Conditions

$u = 0.$ $\left[\frac{m}{s}\right]$

$v = 0.$ $\left[\frac{m}{s}\right]$

$\rho = 1.225$ $\left[\frac{kg}{m^3}\right]$

$p = 1.013 \times 10^5$ $\left[\frac{N}{m^2}\right]$

$\gamma = 1.4$

4. Products of Combustion at the Muzzle:

$u = 1.212 \times 10^3$ $\left[\frac{m}{s}\right]$

$v = 0.$ $\left[\frac{m}{s}\right]$

$\rho = 4.095 \times 10$ $\left[\frac{kg}{m^3}\right]$

$p = 4.853 \times 10^7$ $\left[\frac{N}{m^2}\right]$

$\gamma = 1.24$

5. The Material Constants for the Tube Walls in HELP

$Y_o = 2.1 \times 10^8$ $\left[\frac{N}{m^2}\right]$

Rigidity Modulus $= 8.0 \times 10^7$ $\left[\frac{N}{m^2}\right]$

Failure Criterion = 0.95

The calculational grid chosen was from the muzzle to a point approximately four calibers downstream and from the centerline two calibers radially. In BLAST twenty mesh points were taken to be inside the barrel. In DORF and HELP, ten by ten and in HEMP five mesh points were alotted for the high pressure gases and the thickness of the barrel was taken as twenty by ten except in BLAST where it was one mesh width thick. The meshes, rectangular in geometry, each measured 0.25×10^{-3}m on a side. The different cell numbers considered were dictated by storage limitation of the BRL computing facility.

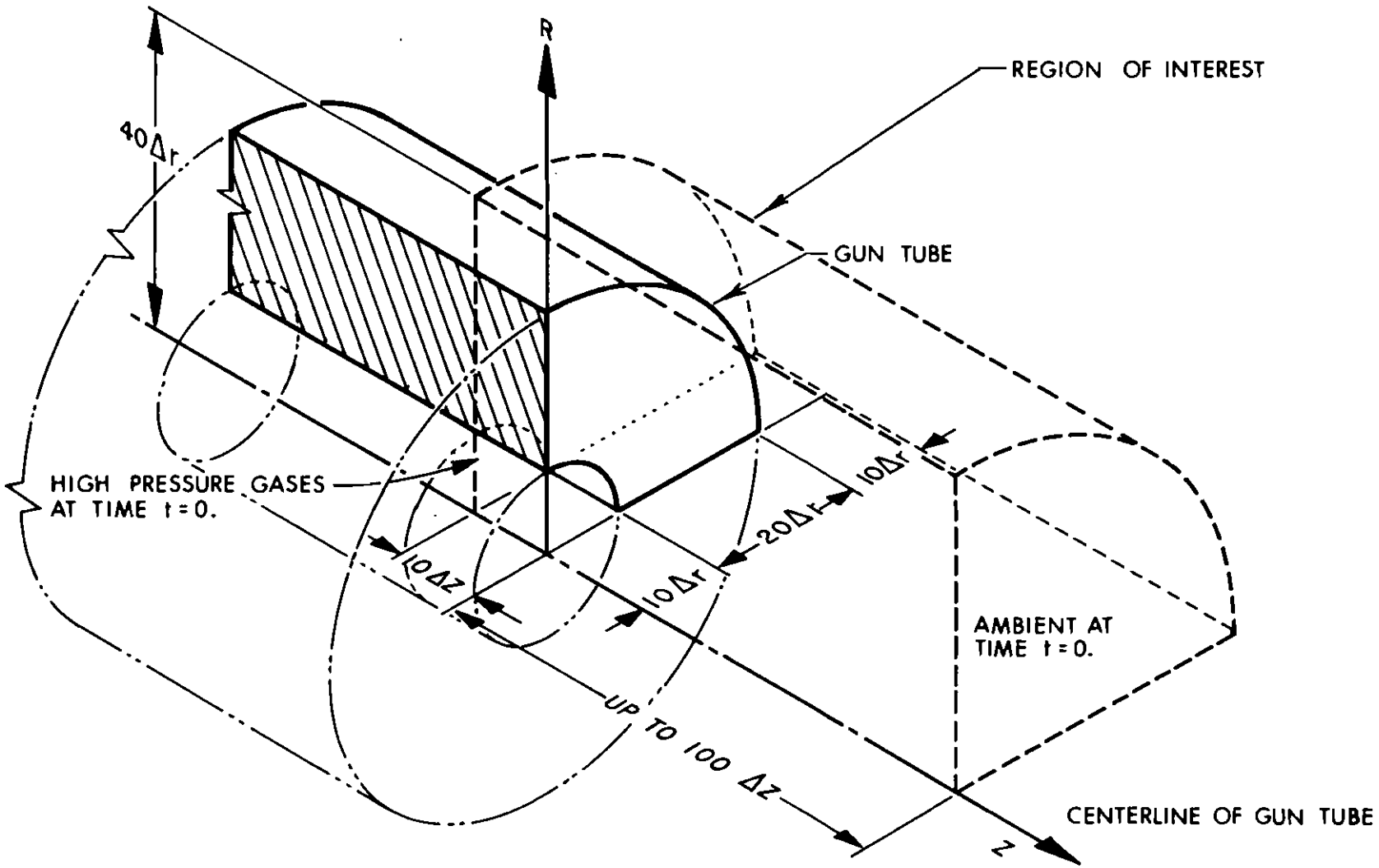

Figure 2. Geometry of the Region of Interest.

TABLE I

SUMMARY OF CODES CONSIDERED

Code Name	BLAST	DORF	HELP	HEMP
Reference	6	8	9	10
Geometry	Axisymmetric	Axisymmetric	Axisymmetric	Axisymmetric Planar
Co-ordinates	Eulerian	Eulerian	Eulerian	Lagrangian
Number of Materials	1	2	15	Multi
Equation of State	Ideal gas	Tillotson Ideal gas	Tillotson	Wide choice available
Artificial Viscosity	No	Available		Yes
Grid Size	110 x 40	80 x 40	40 x 40	20 x 20
Special Feature(s)	Uses Godunov's Method	Strength Option	Tracer Particles Strength Option	Requires Large Storage Strength Option

III. DESCRIPTION OF THE COMPUTER CODES

This chapter outlines the main features of the four computer codes used in the simulation of muzzle blast. For further details the reader is referred to the cited references.

A. BLAST[6]

The computer code BLAST, designed to solve the inviscid, axisymmetric compressible flow equations of a one component gas with a moving boundary representing the projectile, is based on the Godunov difference technique. The advantage of this method is that it can approximate discontinuities with a monotonic profile, but on the other hand, it is only first order accurate. Godunov's scheme consists of two steps. First intermediate values are calculated by solving the Riemann problem for the resolution of a discontinuity, and then the updated values are obtained by leapfrog differencing. In one dimension, then typically,

$$w_m^{n+1} = w_n^n - \frac{\Delta t}{h}\left(f_{m+1/2}^{n+1/2} - f_{m-1/2}^{n+1/2}\right) \tag{6}$$

where w and f are vectors and n+1/2 represents the intermediate time level. The stability restriction,

$$\sigma = \frac{\Delta t}{h}(u+c)_{max} \leq 1 \tag{7}$$

is the usual Courant condition.

In BLAST there is an innovation to this technique. Using the idea of splitting due to Yanenko, instead of solving a two dimensional problem, two one dimensional problems are solved. That is, the idea is to integrate one set of equations, starting with a prescribed set of initial conditions for a half time step along one of the co-ordinate directions. Then, using these results as initial conditions, the second set of equations is integrated in the other co-ordinate direction during the second half time step. One of the advantages derived from this method is that proven, high order explicit numerical schemes developed for one dimensional unsteady flow equations can be used for the integration.

To start the calculation conditions within the barrel are prescribed to be the same as those existing just as the projectile exits the barrel. The gas was taken to be ideal and with γ constant. At the solid boundaries, the normal velocity is set equal to zero. The downstream boundary is expanding just ahead of the blast wave up to an adjustable limit. Past this point, the gas is allowed to 'flow through" the boundary. There is no flow allowed across the center line of the tube. The program contains the option of the presence of a projectile moving at a constant velocity.

B. DORF[9]

This code was developed for hypervelocity impact calculations, but is general enough to permit purely hydrodynamic flow simulation. It consists of two parts: TCLAM, the generator code and DORF where the actual calculations are carried out.

Both of these codes were written for cylindrical geometry with the left hand boundary being the axis of symmetry. The region of interest is subdivided into cells with particles assigned to each. The particles are proportional to the densities and energies such that, for example, the total mass is determined by summing all the particles. This version of the code can handle two different materials.

TCLAM sets up the problem. This involves specifying the geometry, grid dimensions and initialization of the variables. In addition, tracer particles are defined, if used, and constants for the density, internal energy and velocity curve fits are given.

In DORF, the maximum grid can not exceed (IMAX) (JMAX) $\leq$ 4200. Inside this grid there is an active grid consisting of that part of the problem where there is actual movement of mass or internal energy. The calculation is done in two steps. The first step solves the momentum and energy equation as a function of the pressure forces. In the next phase the transport terms, omitted from the first phase are approximated by transporting mass, momentum and energy across the cell boundaries.

The finite difference form of the conservation laws are as follows: The radial momentum equation,

$$\rho_k = \frac{\partial u_k}{\partial t} = \frac{P_{kL} - P_{kR}}{2\Delta r_k} \tag{8}$$

where the subscript kL (kR) indicates the state to the left (right) of the cell under investigation and Δr_k is the cell size of the k-th cell in the r direction. Analogously, for the axial momentum

$$\rho_k \frac{\partial v_k}{\partial t} = \frac{P_{kB} - P_{kA}}{2\Delta z_k} \tag{9}$$

There subscript A(B) designates the cell above (below) the k-th cell and ΔZ_k is the cell dimension in the z-direction. The change in the specific internal energy is then,

$$\rho_K \frac{\partial I_k}{\partial t} = -p_k^n \left[\frac{1}{2\Delta z_k}\left(v_{kA}^1 - v_{kb}^1\right) + \frac{1}{2r_k \Delta r_k}\left(r_k u_{kR}^1 - r_{kL} u_{kL}^1\right)\right] \tag{10}$$

where

$$u_k^1 = 1/2\ (u_k^{n'} + u_k^n). \tag{11}$$

and n' stands for the changes due to pressure forces only. The left hand sides of the equations are differenced in the conventional manner, i.e.,

$$\frac{\partial I_k}{\partial t} = I_k^{n'} - I_k^n \text{ etc.} \tag{12}$$

The solution of the energy equation requires the velocities at two different time steps so that two passes through the first phase of the calculation are required. The first pass integrates the momentum equations and and using the old velocities obtains preliminary interface velocities. The second phase bypasses the momentum equations and computes the new interface velocities. Details are given in reference 9.

The DORF code admits two types of boundary conditions: reflective or transmittive. The left boundary, the axis of symmetry, is always reflective, no flow being allowed across it. The top is always transmittive while the bottom can be either reflective or transmittive.

Upon completion of the first phase of the calculation, involving the momentum and energy equations, the second phase is executed. Here, the transport terms omitted in phase one are approximated by transporting mass across the cell boundaries. This entails, of course, transfer of momenta and energy.

The conservation of mass, in finite difference form is

$$\rho_k^{n+1} = \rho_k^n + \Delta t \left[\frac{2 r_{kL} \rho_{kL} u_{kL}}{(r_{kL} + r_k)\Delta r_k} - \frac{2 r_k \rho_k u_k}{(r_k + r_{kL})\Delta r_k} + \right.$$

$$\left. + \frac{\rho_{kB} v_{kB} \rho_{kk}}{\Delta z_k} \right] \tag{13}$$

Weighting of the velocity in the mass flux equation must be used. DORF performs this in the manner indicated in figure 3.

Assuming flow from left to right, the mass that crosses surface i is that between i and ii. Let Δ = i-ii = $u^{n'}$ t with $u^{n'}$ being the weighted velocity in Δ. Upon expanding the expression for the mean velocity u_i

$$u_i = 1/2\ (u_k + u_{k+1}) \tag{14}$$

in a Taylor series about i-Δ, the following expression is obtained

$$\frac{\Delta}{\Delta t} = u^{n'} \left[\frac{0.5\ (u_k + u_{k+1})}{\frac{\Delta t}{\Delta x}\ (u_{k+1} - u_k) + 1} \right] \tag{15}$$

ρ_k is used in the mass flux equation if in the above expression, equation (15) $(u_k + u_{k+1}) > 0$, otherwise ρ_{k+1} is used.

One can expect flux of mass, momentum and energy across all four sides of a cell. The new velocities and internal energy is the difference that was there before and after the movement. Also, after the fluxes have been determined, it must be ascertained how much of each material moved. The different approaches are again given in the cited reference.

The direction of sweep for the numerical integration is important because it can yield preferential mass treatment depending on whether rows or columns are swept first. This problem is eliminated by a scheme of "looking ahead". For details see reference 9.

The time step for the integration is determined, as in the PIC method, being based on the particle velocity. Again, it is the Courant condition that must be satisfied. Finally, the equation of state used is the one due to Tillotson. See the discussion of the HELP code for particulars.

DORF contains an artificial viscosity subroutine, which may be called, as needed. The code also has a Lagrangian feature incorporating tracer particles. Their motion is determined by using the velocities, pressure and energies obtained in the calculation. Thereis no influence on the hydrodynamics from the tracers, but the tracers give a good idea of the development of the flow field.

C. HELP[9]

HELP is a two dimensional, axisymmetric, Eulerian code developed for solving hydrodynamic elastic-plastic flow problems. The algorithm was derived from the particle in cell (PIC) method with the discrete particles replaced by a continuum to allow the treating of small compressions without the need to resort to too many particles. The version available to us was limited to only one material.

The differential equations expressing the conservation laws are replaced by analogous integral equations obtained by integrating over a cell volume V, followed by the conversion of the volume integral of divergences to surface integrals over the cell surface yielding

$$\frac{\partial}{\partial t}\int_V \rho dV = -\int_S \rho u_i n_i ds \tag{16}$$

$$\frac{\partial}{\partial t}\int_V \rho u_j dV = \int_S \sigma_{ij} n_i ds - \int_S \rho u_i u_j n_i ds \tag{17}$$

$$\frac{\partial}{\partial t}\int_V \rho E_T dV = \int_S \sigma_{ij} u_j n_i ds - \int_S \rho u_i E_T n_i ds \tag{18}$$

The difference analogs are explicit and accurate to terms of first order. The calculation proceeds in phases:

Phase I Acceleration of the material in a cell due to pressure and the deviatoric stress gradients across the cells are calculated.

Phase II Updated velocities are used to transport the appropriate amount of mass, momenta and internal energy across each cell boundary and the revised cell quantities are computed.

Phase III The deviator stresses acting on each cell edge and the hoop stresses are determined here. For the gas phase this step is bypassed.

In the multi-material version of the code, each material is circumscribed by a series of massless tracer particles which are propagated at the local average velocity for the continuum. At the boundaries and material interfaces diffusion is prevented by employing Lagrangian techniques.

HELP uses the Tillotson equation of state

$$p = \left[a + \frac{b}{\frac{I}{I_o \eta^2} + 1}\right] I\rho + A\mu + B\mu^2 \tag{19}$$

where a = material constant
b = material constant
$\eta = \frac{\rho}{\rho_o}$
A = material constant
B = material constant
$\mu = \eta - 1$
I = specific internal energy
ρ = mass density

A is equal to ρ_o C where C is the speed of sound and ρ_o the zero pressure density, a is the asymptotic Gruneisen coefficient and b equals G_o-a with G_o the zero pressure Gruneisen parameter. B is so chosen as to fit the experimental data.

The deviatoric stress increments dS_{ij} are determined by the elastic relation

$$dS_{ij}' = 2Gd\varepsilon'_{ij} \tag{20}$$

where G is the modulus of rigidity and $d\varepsilon_{ij}'$ is the increment in the deviatoric strain.

For air, a γ-law equation of state in the form

$$p = (\gamma-1)\rho E \tag{21}$$

where E is the specific internal energy, is used.

The code has a variable zoning option as well as a rezoning feature. The latter can be useful to eliminate oscillations when a shock passes through a transmittive grid boundary. The boundaries require special treatment because quantities are not defined for cells outside the grid. One may specify a transmittive boundary at the top and right of the grid and either transmittive or reflective boundary at the axis. At border cells boundary conditions are specified by assuming imaginary cells outside the grid. If the boundary is transmittive, the imaginary cell has the same variable values as the border cell while for a reflective boundary, the states, save for a sign of the normal velocity component, are the same.

Stability is ensured by using for Δt the minimum value, over all cells, of the smallest cell's dimension divided by the sum of the cell's maximum velocity component and its sound speed.

D. HEMP[11]

Of the four codes tried in this simulation, only HEMP is Lagrangian. It was intended for dynamic plasticity investigations, but has also been used for flow simulation[12]. This is an extremely versatile code, especially with regard to treating solid deformations, and even includes a combustion option. A wide variety of equations of states is available including those for gases. The code includes an artificial viscosity so that developing shocks are treated automatically in the course of computation.

Much of the innovation in HEMP concerns the treatment of strength of materials effects. These are of no interest for our simulation. Below, we summarize some of the salient features of the code relevant to the hydrodynamic calculations.

The scheme for mass zoning is shown in figure 4. Basically, the material is divided into quadrilaterals with a grid j-k that moves with the material. The mass at time zero of each quadrilateral is obtained as the product of the initial density and volume swept out by the quadrilateral rotated about the x-axis. Thus for quadrilateral 1

$$M_1 = 1/3 \left(\frac{\rho^{\bullet}}{V^{\circ}}\right)_1 \left[(y_2^{\circ} + y_3^{\circ} + y_4^{\circ})\, A_a + (y_1^{\circ} + y_2^{\circ} + y_4^{\circ})\, A_b^{\circ}\right]_1 \tag{22}$$

A_a is an area and is determined from

$$(A_a)_1^n = 1/2 \left[x_2^n (y_3^n - y_4^n) - x_3^n (y_4^n - y_2^n) + x_4^n (y_2^n - y_3^n)\right] \tag{23}$$

and analogously for A_b.

The conservation of mass then reads as

$$V_1^n = 1/3 \left(\frac{\rho}{M}\right)_1 \left[(y_2^n + y_3^n + y_4^n)\, A_a^n + (y_1^n + y_2^n + y_4^n)\, A_b^n\right]_1 \tag{24}$$

$$V_1^n = \left(\frac{\rho^{\circ}}{\rho^n}\right)_1 \tag{25}$$

The equation of motion in the x-axial direction is

$$\begin{aligned} \dot{x}_{j,k}^{n+1/2} = \dot{x}_{j,k}^{n-1/2} - \frac{\Delta t^n}{2\phi_{j,k}^n} \Big[& (\Sigma_{xx})_1^n (y_{II}^n - y_{III}^n) + (\Sigma_{xx})_2^n (y_{III}^n - y_{IX}^n) \\ & + (\Sigma_{xx})_3^n (y_{IV}^n - y_I^n) + (\Sigma_{xx})_4^n (y_I^n - y_{II}^n) - (T_{xy})_1^n (x_{II}^n - X_{III}^n) \\ & - (T_{xy})_2^n (X_{III}^n - X_{IV}^n) - (T_{xy})_3^n (X_{IV}^n - X_I^n) - (T_{xy})_4^n (x_I^n - X_{II}^n)\Big] \\ & + \Delta t^n (\alpha)_{j,k}^n \end{aligned} \tag{26}$$

and analogously for the y-direction. For explanation of subscript notation see Figure 4.

The internal energy, E is determined from

$$\tilde{E}_1^{n+1} = \left[E^n - (P^n + \bar{q})\, (V^{n+1} - V^n) + \Delta z^{n+1/2}\right] \tag{27}$$

where Δz is the change in distortion energy.

$$\tilde{P}_1^{n+1} = P(\tilde{E}^{n+1}, V^{n+1})_1 \tag{28}$$

$$E_1^{n+1} = \left[\tilde{E}^{n+1} - 1/2(\tilde{P}^{n+1} - P^n)(V^{n+1} - V^n)\right]_1 \tag{29}$$

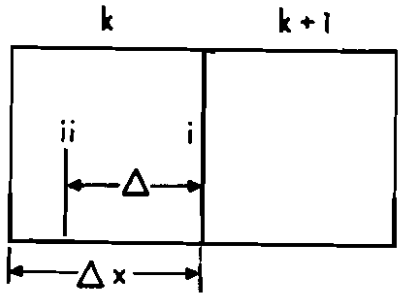

Figure 3. Scheme of Velocity Weighting Used in DORF.

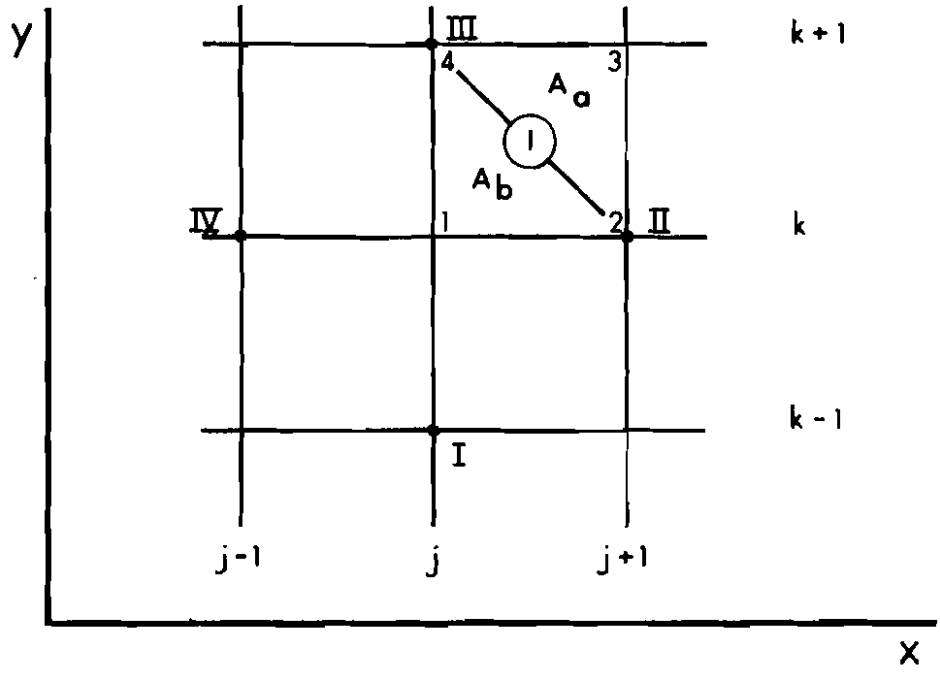

Figure 4. The Layout of the Computational Grid of the HEMP Code.

$$P_1^{n+1} = P(E^{n+1}, V^{n+1})_1 \tag{30}$$

The artificial viscosity q is given by

$$q_1^{n+1/2} = \left[\frac{C_o^2 \rho_o A^{n+1/2}}{V^{n+1/2}} \left(\frac{\dot{V}}{V}\right)^2\right]_1 \tag{31}$$

where $C_o^2 = 4$.

Boundaries are treated by reflection, using imaginary cells and the stability condition is that derived by von Neumann and Richtmyer. The version of the code at our disposal does not have the capability to rezone automatically, nor to indicate degenerate cells.

IV. CALCULATIONAL RESULTS

A. Criteria for Evaluation

Ideally, computational results should be compared with experimental observations. Due to the extreme flow conditions present at the muzzle of a gun, only a limited amount of such data is available [13,14]. Essentially these are photographic records, including shadowgraphs, at preselected time intervals or overpressure measurements downstream of the muzzle.

Therefore, we compare our results with photographs of firings of an M-16 rifle at several times paying particular attention to

1. the shape of the flow field
2. location of the shocks
3. velocity of the shocks

In addition, we compare the codes among themselves, for costs, that is how much computer time does it take for a certain real time to be simulated and how much storage is required.

As a further check, we compare the computational results with the prediction of blast wave theory[15] and steady jet theory[16]. The latter gives shock, Mach disk locations and the geometry of the jet such as L/D ratios. Since these are only valid for steady flow, the conclusions must be interpreted carefully.

Under the conditions of isentropic flow, Crist et al[16], give the following relationship for the position of the Mach disk X_m, as a function of the pressure ratio.

$$\frac{P}{P_\infty} = 2.4 \left(\frac{X_m}{D}\right)^2 \tag{32}$$

There P_∞ is ambient pressure and D represents the sonic nozzle exit diameter. For M_x, the Mach number upstream of the shock, much greater than one and using the relationship between the stagnation pressure and Mach number as well as the relationship between static pressure behind and before the normal shock and Mach number, one obtains

$$\frac{X_m}{D} \simeq M_x^{\frac{1}{\gamma-1}} \left[\left(\frac{\gamma-1}{2}\right)^{\frac{\gamma}{\gamma-1}} \frac{\gamma+1}{4.8\gamma}\right]^{1/2} \tag{33}$$

Again, it should be kept in mind that the derivations are for steady flow conditions of an underexpanded jet.

As an order of magnitude check on the location of the blast wave as a function of time and energy deposition, we use the estimate given by Sedov[15]. Under cylindrical symmetry, the shock wave co-ordinate R, measured from the point of explosion, as a function of time, is given by

$$r = \left(\frac{E}{\rho}\right)^{1/5} (t)^{2/5} \tag{34}$$

where t is the elapsed time and E the energy per unit volume deposited into the flow.

Finally, at early times empirical correlations[1] show that the pressure profile at the muzzle may be expressed as,

$$p = p_1 e^{-t/t_1} \tag{35}$$

where

$$p_1 = 0.598 \times 10^8 \left[\frac{N}{m^2}\right]$$

$$b_1 = 0.526 \times 10^{-3} [s]$$

B. Results

Under the initial conditions summarized in Chapter II, the four codes were run up to five hours of machine time or until the code got into trouble, whichever occurred first. The results are summarized below.

First, some general remarks. The calculations were started in a shock tube fashion, that is, the end of a tube containing high pressure gases was exposed to the ambient at the time zero. However, we assumed the combustion gases throughout the tube, at time t=0, to possess a uniform, finite velocity corresponding to real muzzle conditions at the time the projectile completely clears the gun tube. This in contrast to the real process where the moving projectile in the tube compresses a column of air ahead of it leading to the first shock observed on the photographs. Also, combustion gases leak around the projectile leading to the precursor blast wave.

In addition, by excluding the presence of the projectile, the calculated flow field, of necessity, deviates from the photographs of actual firings. This includes the rearward facing bow shock at the base of the projectile and at early times, the region of the intense shock interaction.

In the figures the shock was located at the point of steepest gradient in the pressure profile. Admittedly, this is somewhat arbitrary in view of the fact (see figure 5, for example) that the shock is spread over up to 10 mesh widths in the calculations, but alternative criteria, are no more accurate.

The contour plots (figures 11-12) suggest the location of the starting vortex at the lip of the gun tube. This is also apparent from the velocity plots (figures 8-10) as one proceeds laterally or radially from the muzzle.

None of the calculated results showed the presence of the Mach disk. In case of the BLAST code, for t>1.58μs, due to the subsonic throat conditions, the disk is not expected on physical grounds. Also, for these times, the steady state formula(32) would place it at a position to which the flow has not, as yet, penetrated.

1. BLAST

The BLAST code was run out to 400 time cycles corresponding to 20.8μs real time. The run took 300 minutes on BRLESC II.

The computational results are illustrated in the (a) portion of figures 5 to 10 where pressure, axial and radial velocity as a function of distance along the tube's center line, at forty five degrees to the muzzle and ninety degrees to the muzzle, all measured from the axis of the tube at the muzzle, are plotted. Each of the diagrams shows curves corresponding to the labeled real times. Figure 16 gives the shock location as a function of time. Curves of constant pressure at succeeding times is illustrated in figure 11. Shock velocity was observed to vary between $5.755 \times 10^3 [\frac{m}{s}]$ at 3μs down to about $3.28 \times 10^3 [\frac{m}{s}]$ at 8μs. It should be noted that the barrel thickness in BLAST is only one mesh width in contrast to the other codes.

As expected, plots show a decay in the flow variable amplitudes as one proceeds away from the muzzle. However, the shape of the flow field, except for the bow shock deviates appreciably from the photograph of the flow field given in figure 1. Note especially the lateral boundary of the jet close to the tube. Instead of the expected sidewise expansion, the jet remains of roughly constant cross sectional area for a few calibers downstream. Also, the computational results do not reveal the presence of the Mach disk, triple point or the contact surfaces. Thus significant flow details are missing from the computer results. In view of storage and running time limitations, 22 mesh widths were alotted to the gun tube length containing the high pressure gases. Due to the emptying of the barrel, it was found that at 1.50μs the Mach number at the throat was 1.165 but already at 2.97μs it dropped down to 0.787 and stayed below 1 for all times thereafter. Thus, for a realistic simulation a much larger barrel should be considered. This, of course, necessitates the availability of a computer with a large memory.

The blast wave location according to equation (34) at time 4μs should have been at 0.60×10^{-2}m from the muzzle while BLAST gave its location at 1.75×10^{-2} m. Photographic evidence puts it at 0.75×10^{-2}m. Thus there is a deviation of 133% between the calculated and observed values. There is qualitative agreement between these results and those reported by Spong[17] though the latter worked at considerably lower pressure levels.

2. DORF

The best results were obtained from the computer code DORF. The flow shape, pressure and velocity history, and flow detail were the most reasonable from these runs. To simulate 8μs real time, five hours of running time of BRLESC II was required.

Our results are illustrated in the b portion of figures 5 through 11. Again we plot pressure, axial and radial velocity as a function of distance along the gun tube's axis, at forty five degrees and at ninety degrees to the muzzle, starting at the muzzle. Each of the curves corresponds to the real time indicated. Figure 12 gives pressure contours at times corresponding to those of the BLAST calculations enabling a comparison to be made between the results of the two codes. Note that due to the shortness of the barrel, as the slug of gas clears the barrel there occurs an appreciable pressure drop at the muzzle. This is noticeable for times greater than 3.7μsec. Finally, figure 16 shows the shock location as a function of time as calculated by BLAST and DORF.

The shock velocity was observed to vary between $3.546 \times 10^3 [\frac{m}{s}]$ at 3.5μs down to $2.614 \times 10^3 [\frac{m}{s}]$ at 6.5μs. The other flow variables showed analogous attenuation. The contour plots indicate the formation of the starting vortex at the lip of the muzzle. A finer mesh spacing would be required to obtain more detail on the vortex dynamics. The Mach number at the throat of the muzzle ranged from $M_x=0.725$ at 1.59μsec to $M_x=0.716$ at 7.36μsec.

A comparison between figures 1 and 12 shows that the calculated flow shape is quite reasonable and figure 16 indicates that the shock velocity is close to the values predicted by BLAST but deviates somewhat from experimental values. On the other hand, we were unable to show the presence of the Mach disk or any of the slip lines within the flow.

With only ten mesh points alloted to the high pressure combustion gas reservoir, the tube emptied too fast as evidenced in the contour plots at times greater than 3μsec. This accounted for the Mach number drop at the muzzle and the rapid change in the flow variables at the muzzle.

3. HELP

Right from the outset serious difficulties were encountered in running this code. We considered a grid of 40 x 40 points. To be able to run the version of the code available to us, we had to assume that the combustion products and the ambient to be the same gas, but having different internal energies. The tube walls were specified as composed of steel with a yield strength of

$$Y_o = 1.2 \times 10^9 \left[\frac{N}{m^2}\right]$$

and rigidity modulus of

$$G = 8.2 \times 10^7 \left[\frac{N}{m^2}\right].$$

As seen from figure 13b the flow field develops as expected but something strange transpires. Regions of negative pressures and internal energy appear in the solid and in the ambient gas. Material evaporates locally. The computer also gives mixed cells at physically wrong locations. At certain values of the initial internal energy of the solid, the gun tube wall deforms and can even ablate and mix with the gas. The high pressure gas is nowhere near the state where such effects would be expected. Analogous difficulties were encountered at other installations with the code[19].

Several attempts were made to remedy the situation. Strengths and densities several times that of steel were tried but the results were the same. On examining the equations and boundary conditions, one must conclude that probably both are in need of revision. Particularly, reflective conditions should be employed at solid walls, and the strength formulation reexamined. That the shortcomings in the code have not been discovered earlier probably can be ascribed to the fact that HELP has been developed for hypervelocity impact problems where the pressures and energies are of orders of magnitude larger than here. Since the runs with HELP were terminated after only .84 microseconds real time, or 60 minutes machine time, no comparison with experimental data is possible.

4. HEMP

HEMP, the Lagrangian code, was run both on a grid of 40 x 40 and 20 x 20, each $\Delta x = \Delta y = 2.5 \times 10^{-4}$m the smaller region requiring 64K storage. The longest run could simulate up to .9μsec. real time. The code has a built in cutoff. That is, if the determined time step is less than 10^{-4}μsec, it automatically stops. The time step is determined from the ratio of the smallest dimension of the cell to the velocity there scanning the cells. When the grid gets too distorted, as happened in our run, one of the dimension of the cells will usually become rather small, leading to the observed conditions.

A run is illustrated in figure 13. The fatal distortion starts at the lip of the nozzle and gets progressively worse. The arrows are proportional to the velocity vectors and give an idea of the magnitudes of the flow variables. At time .8μsec the shock is at 25 x 10^{-3}m from the muzzle, and the pressure jump is approximately 10. At I = 15, J = 4,* for example near the lip of the nozzle, the originally square cell has been distorted into a narrow rectangular region. At t=.7μsec, near the lower limit of the time step, the x-component of the velocity is 2196 $[\frac{m}{s}]$ while the y-component is 411 $[\frac{m}{s}]$ and the pressure 7.904 x 10^6 $[\frac{N}{m^2}]$. At the throat the Mach number, M_x = 1.38.

Several schemes were tried to improve the results that is, to delay the distortion of the grid at the corner. Reasoning from fluid dynamics, where boundary layers are observed, we put into the row representing the fluid next to the inside wall of the gun and extending out into the ambient a viscosity much greater than that assigned to the other gases. It was our expectation that this would slow the distortion process. Indeed, this was also observed, but it could only prolong the run by a few microseconds real time. The value of the artificial viscosity coefficient used was 60 while the maximum value of q was 1.987 x 10^{-4} $[\frac{N}{m^2}]$. Elsewhere in the flow field, the viscosity coefficient was kept at 4.0.

Since the computational times reached were less than one microsecond before the code exited no comparison with our photographic records was possible. Possibly through a rezoning scheme, the runs could be extended in duration, but it is our opinion, that there is no rational ground to believe that runs of the order of tens of microseconds real time could be achieved. To reach 0.8 microseconds real time, it took a run of 48 minutes on BRLESC II.

V. CONCLUSIONS

Under identical initial conditions, the computer codes BLAST, DORF, HELP, and HEMP have been tested for capability of muzzle blast flow field simulation of a small bore weapon. It has been found that HELP and HEMP are unsuitable for the task.

BLAST is able to simulate the gross features of the flow including the blast wave. However, the shape of the predicted flow field for real times less than 20μs deviates in shape appreciably from the observed. Also, the code is unable to show the Mach disk and the triple shocks known to be present.

---

*I and J are the grid co-ordinates.

DORF can also furnish the global features of the flow field without resolving, for the mesh size chosen, the finer features of the flow. Both DORF and BLAST exhibit order of magnitude agreement with the theoretical predictions of the blast wave velocity and pressure jump based on our criteria given in Chapter IV. Overall, DORF is much better than BLAST. However, to be useful for our purposes, DORF would have to modified to enable it to handle a projectile, that is a moving boundary, as well as sharpen the shock profiles. Such changes are major and would require the expenditure of considerable time and effort. A new code development, possibly along the lines of the flux corrected transport algorithm, appears to be more promising and is the approach that should be pursued.

In conclusion then, we feel that none of the examined codes are good enough as a design aid in the advancement of muzzle device technology.

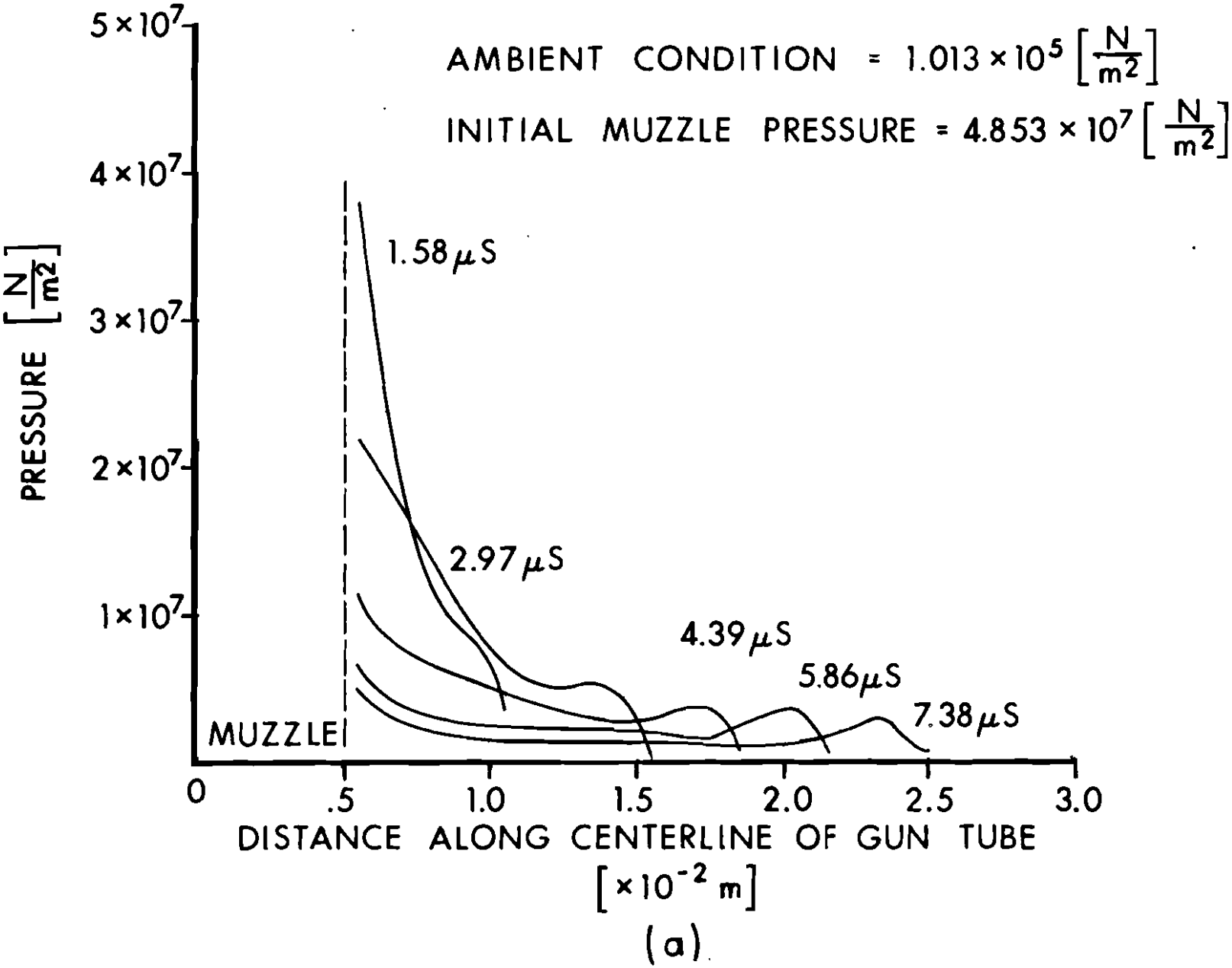

Figure 5. Pressure Versus Distance along the Axis of the Gun Tube.
a. Results from the BLAST Code.
b. Results from the DORF Code.

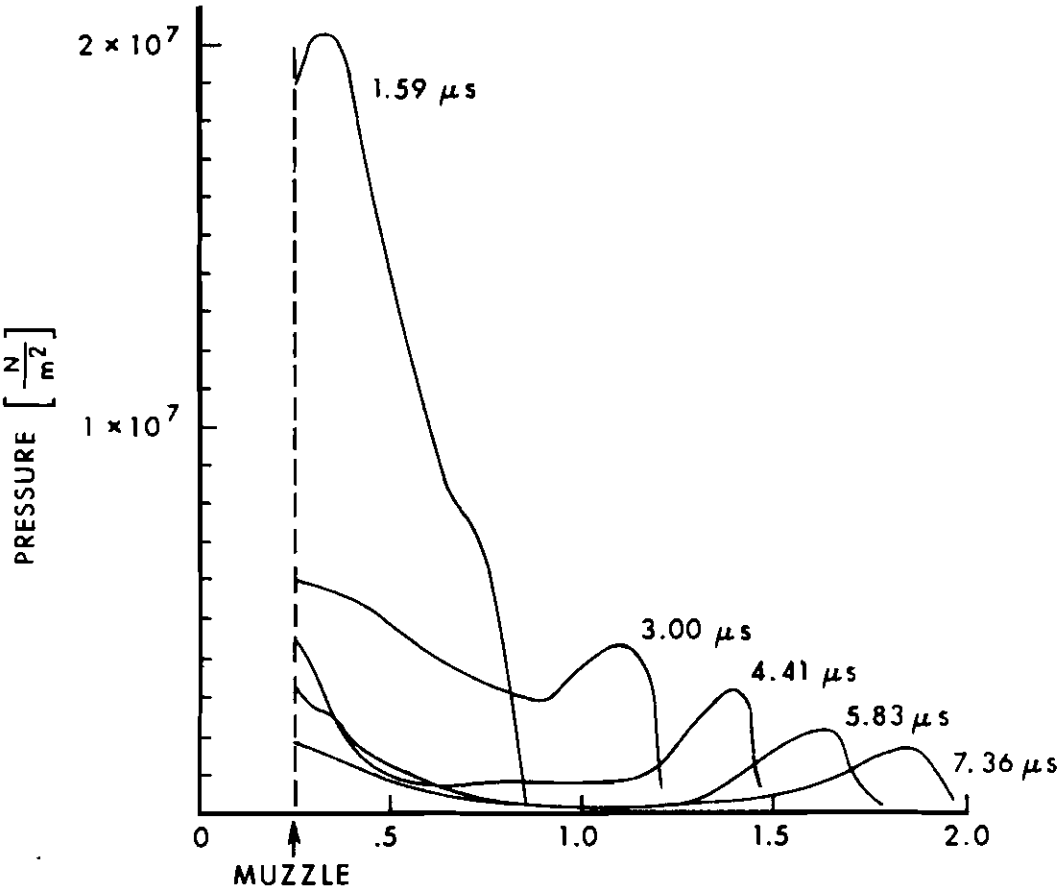
2 × 10^7
1 × 10^7
PRESSURE [N/m^2]
1.59 μs
3.00 μs
4.41 μs
5.83 μs
7.36 μs
0
.5
1.0
1.5
2.0
MUZZLE
DISTANCE ALONG CENTERLINE OF GUN TUBE
[× 10^-2 m]

(b)

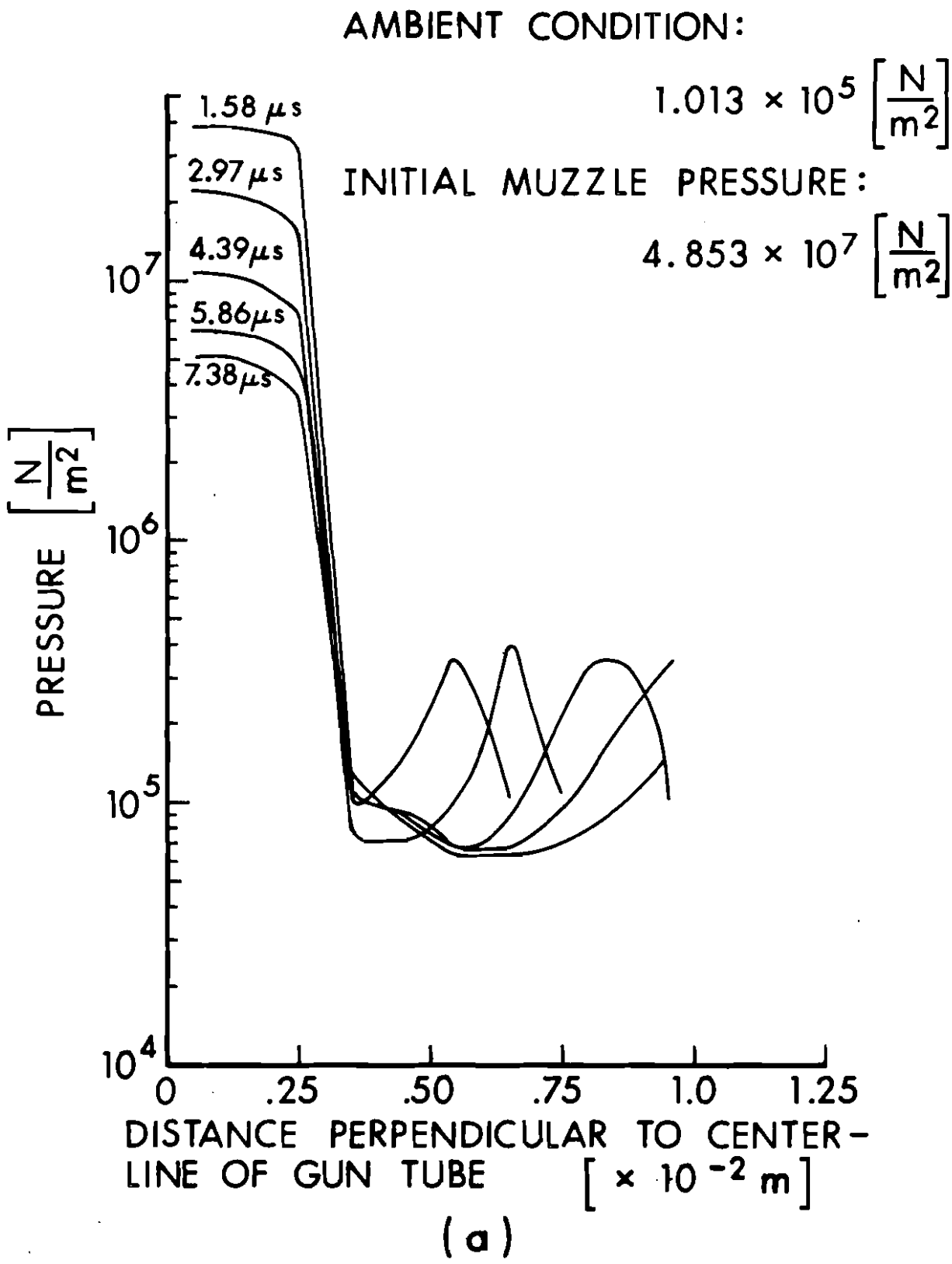

Figure 6. Pressure Versus Distance at 90° from the Axis of the Gun Tube Measured from the Muzzle.
a. Results from the BLAST Code.
b. Results from the DORF Code.

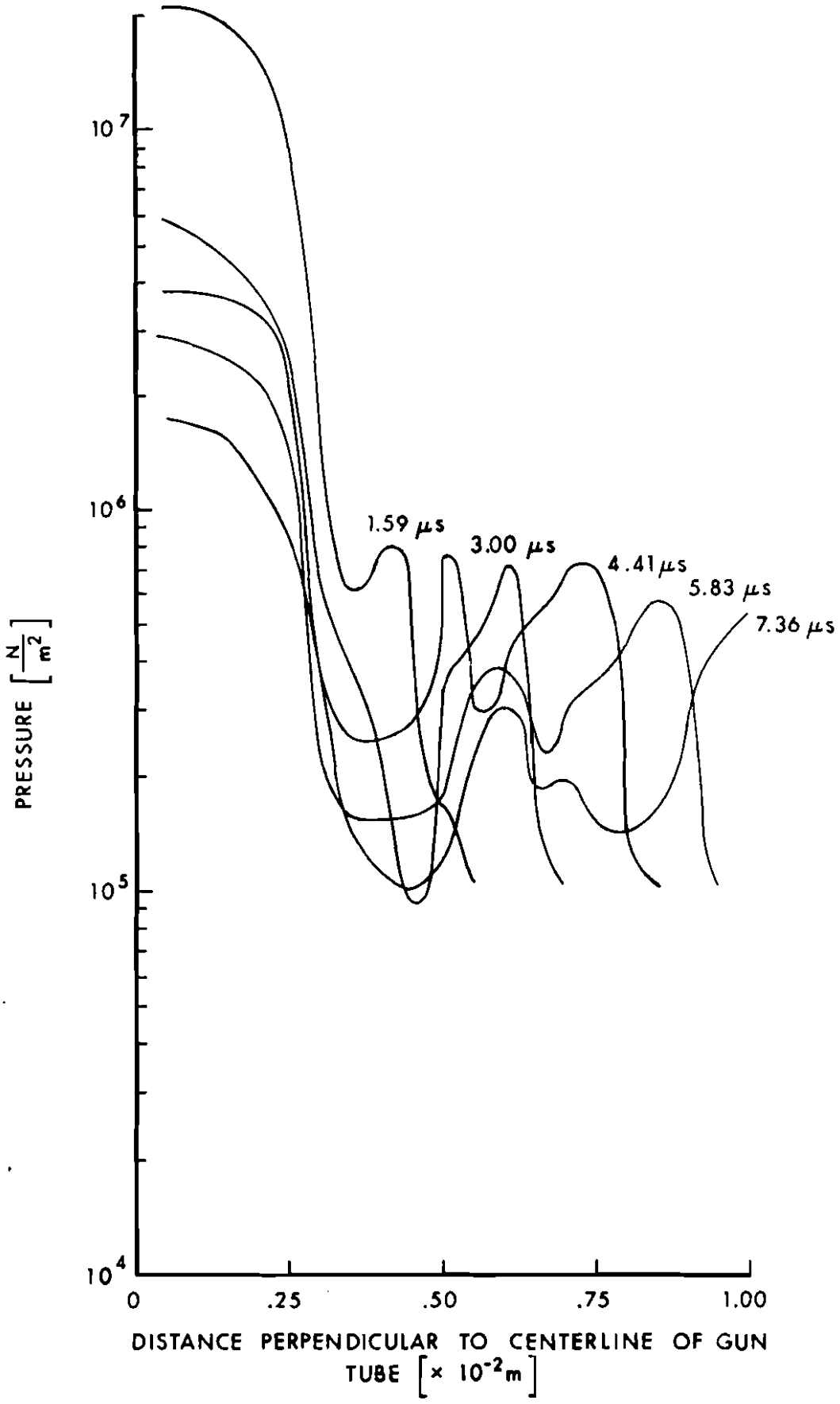
10^7
10^6
10^5
10^4
PRESSURE $\left[\frac{N}{m^2}\right]$
1.59 μs
3.00 μs
4.41 μs
5.83 μs
7.36 μs
0
.25
.50
.75
1.00
DISTANCE PERPENDICULAR TO CENTERLINE OF GUN TUBE $[\times 10^{-2}m]$

(b)

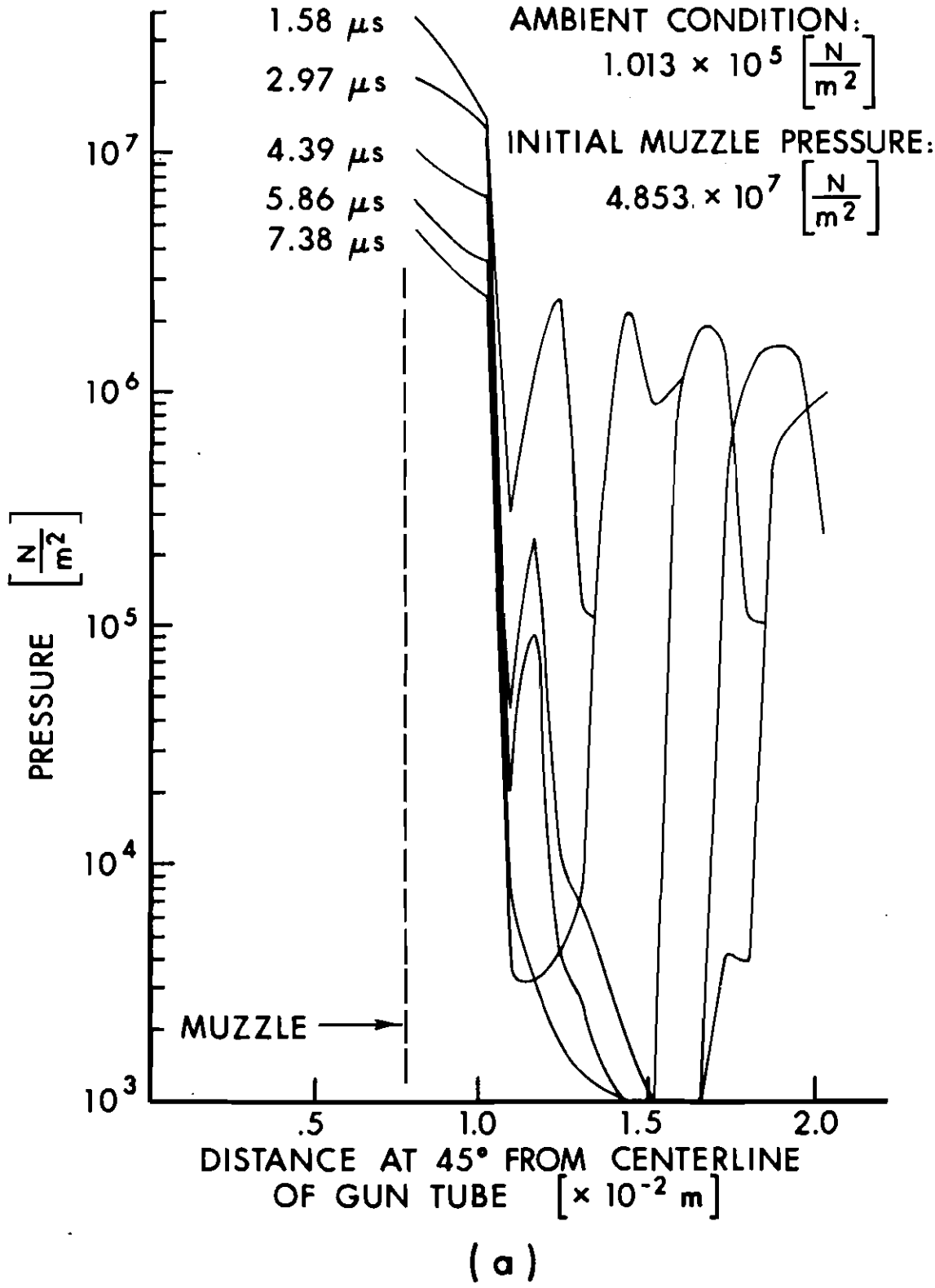

Figure 7. Pressure Versus Distance at 45° from the Axis of the Gun Tube.
a. Results from the BLAST Code.
b. Results from the DORF Code.

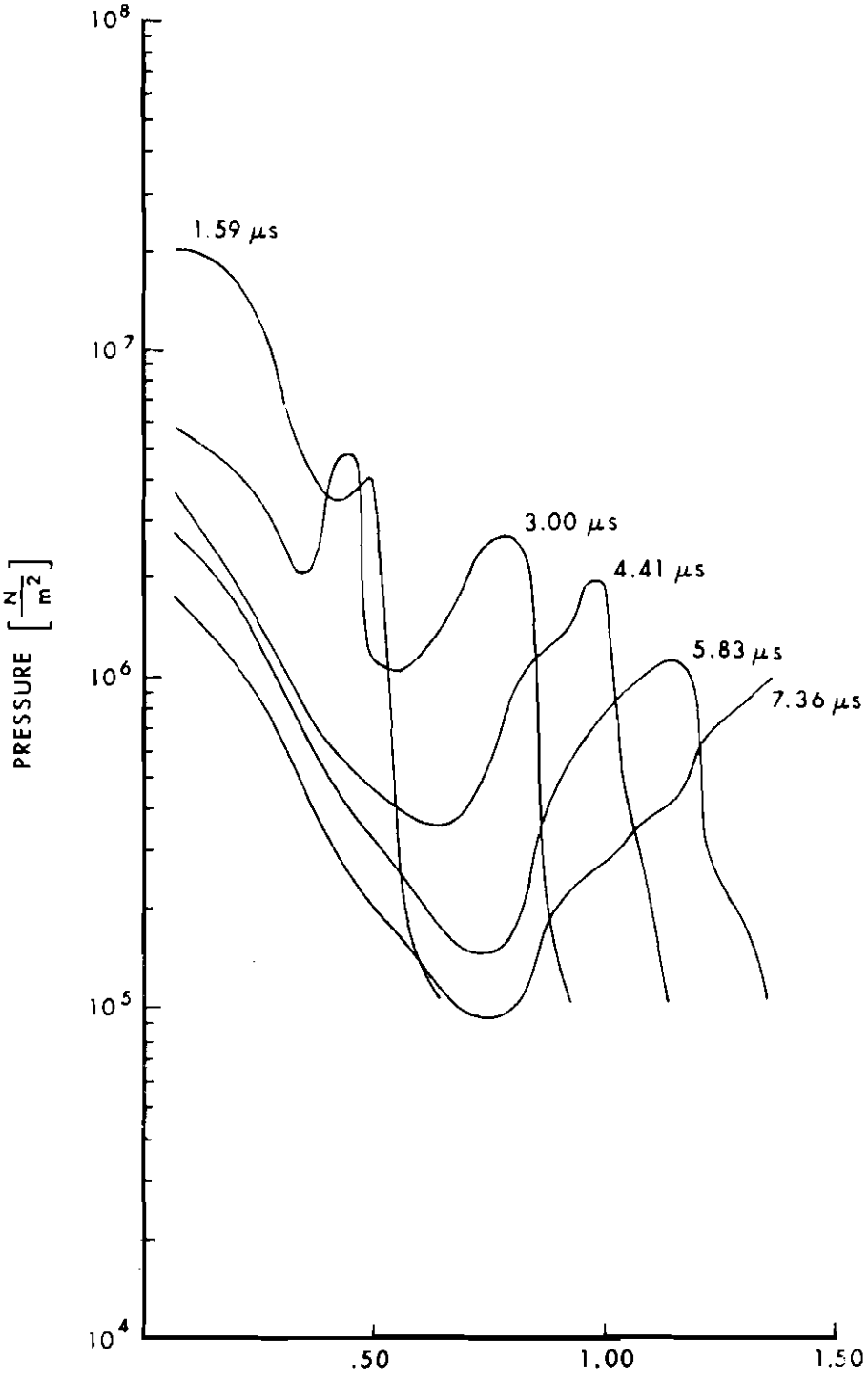
10^8
10^7
10^6
10^5
10^4
1.59 μs
3.00 μs
4.41 μs
5.83 μs
7.36 μs
PRESSURE $\left[\frac{N}{m^2}\right]$
.50
1.00
1.50
DISTANCE AT 45° FROM CENTERLINE OF GUN TUBE
$[\times 10^{-2}m]$

(b)

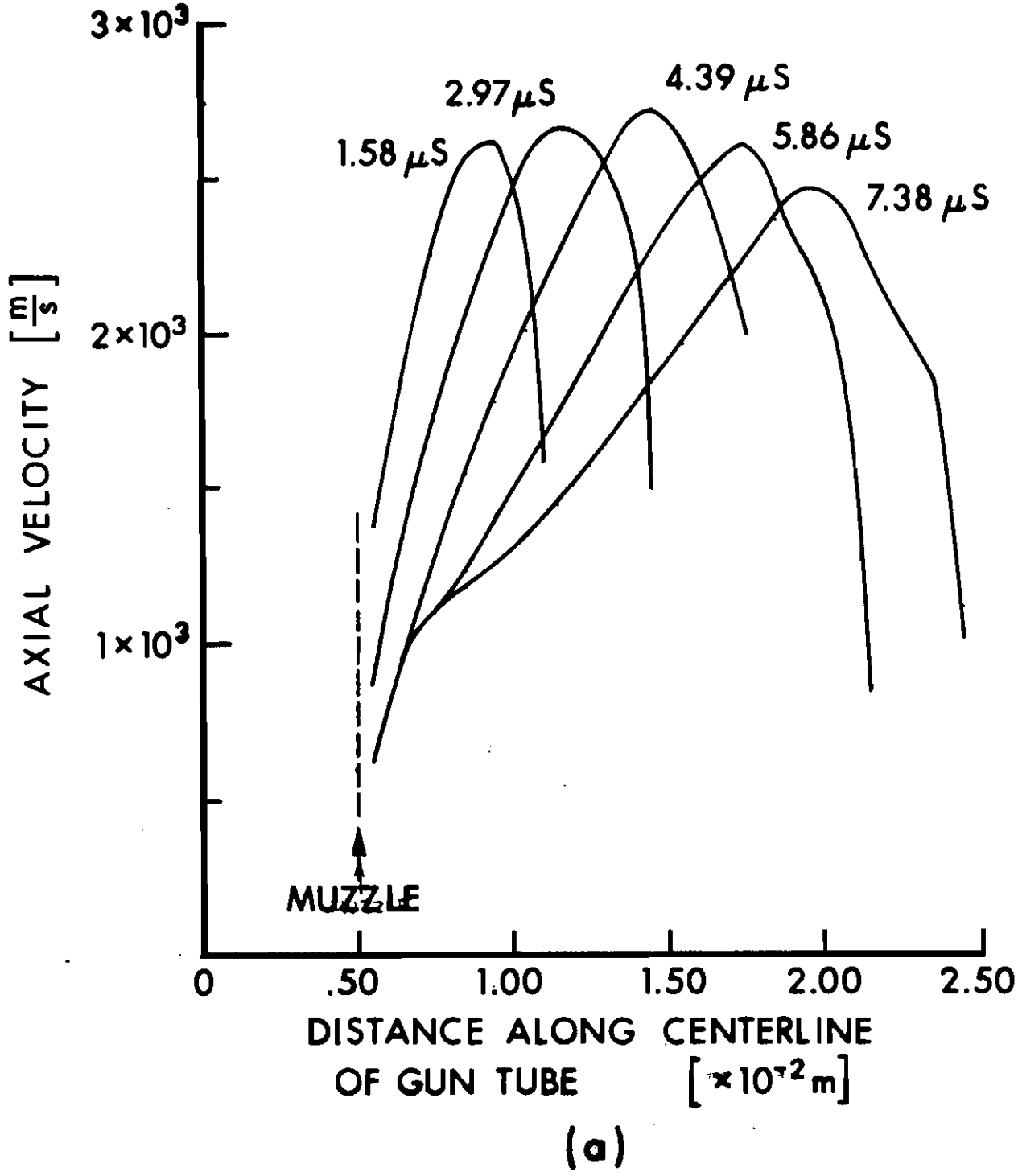

Figure 8. Axial Velocity Versus Distance Along the Axis of the Gun Tube.
a. Results from the BLAST Code.
b. Results from the DORF Code.

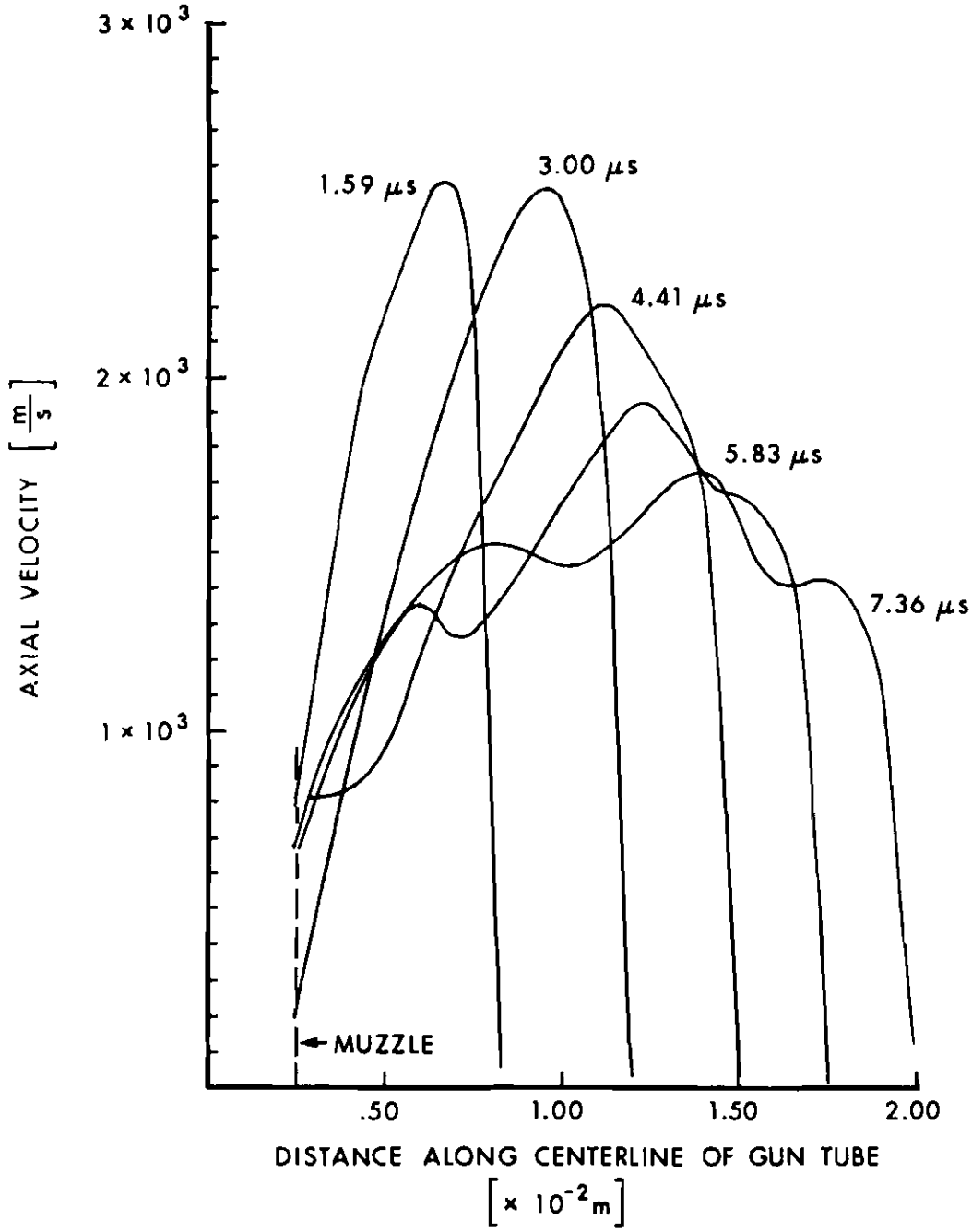
3 × 10^3
2 × 10^3
1 × 10^3
AXIAL VELOCITY [m/s]
1.59 μs
3.00 μs
4.41 μs
5.83 μs
7.36 μs
MUZZLE
.50
1.00
1.50
2.00
DISTANCE ALONG CENTERLINE OF GUN TUBE
[× 10^-2 m]

(b)

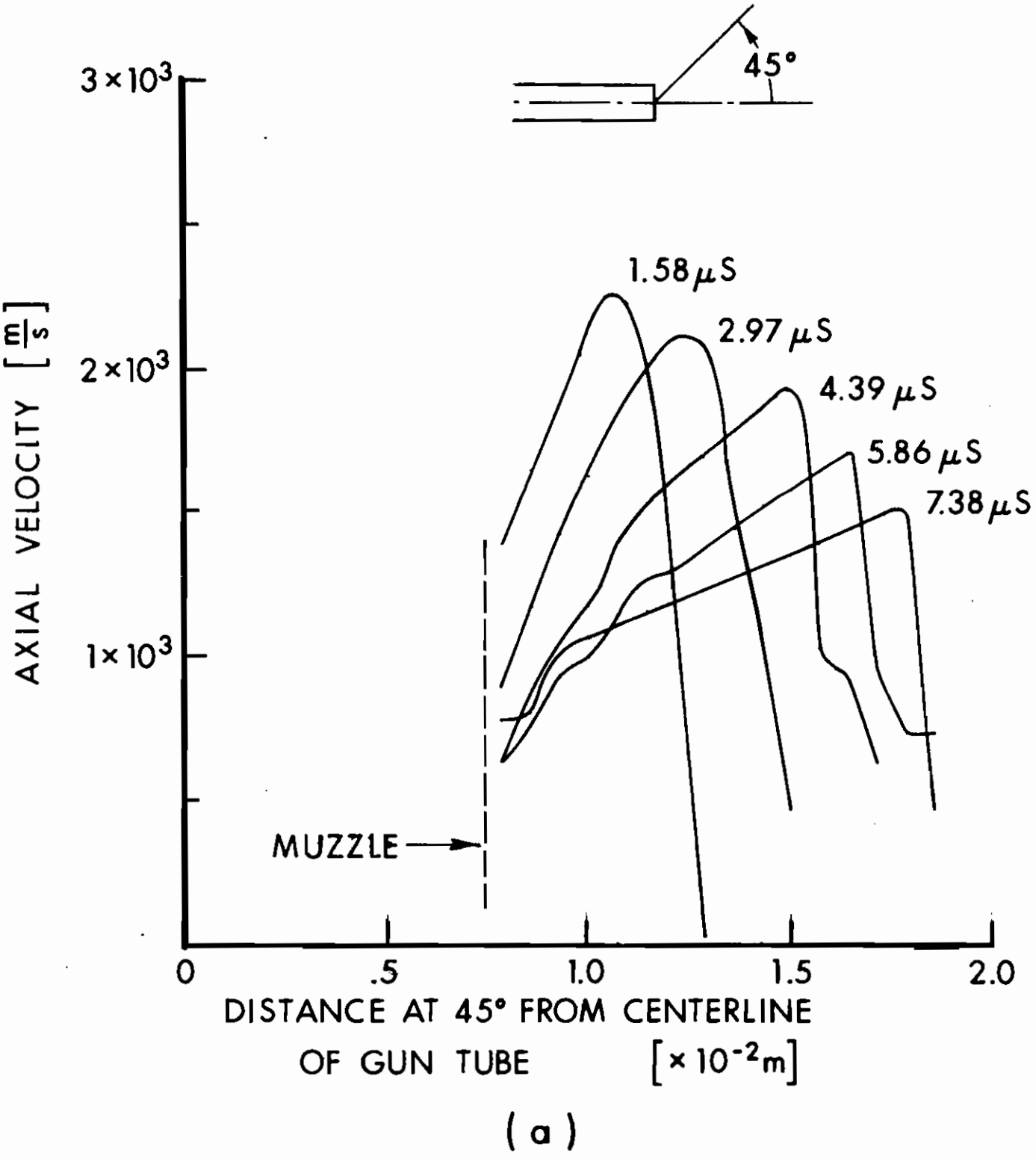

Figure 9. Axial Velocity Versus Distance at 45° from the Axis of the Gun Tube.
a. Results from the BLAST Code.
b. Results from the DORF Code.

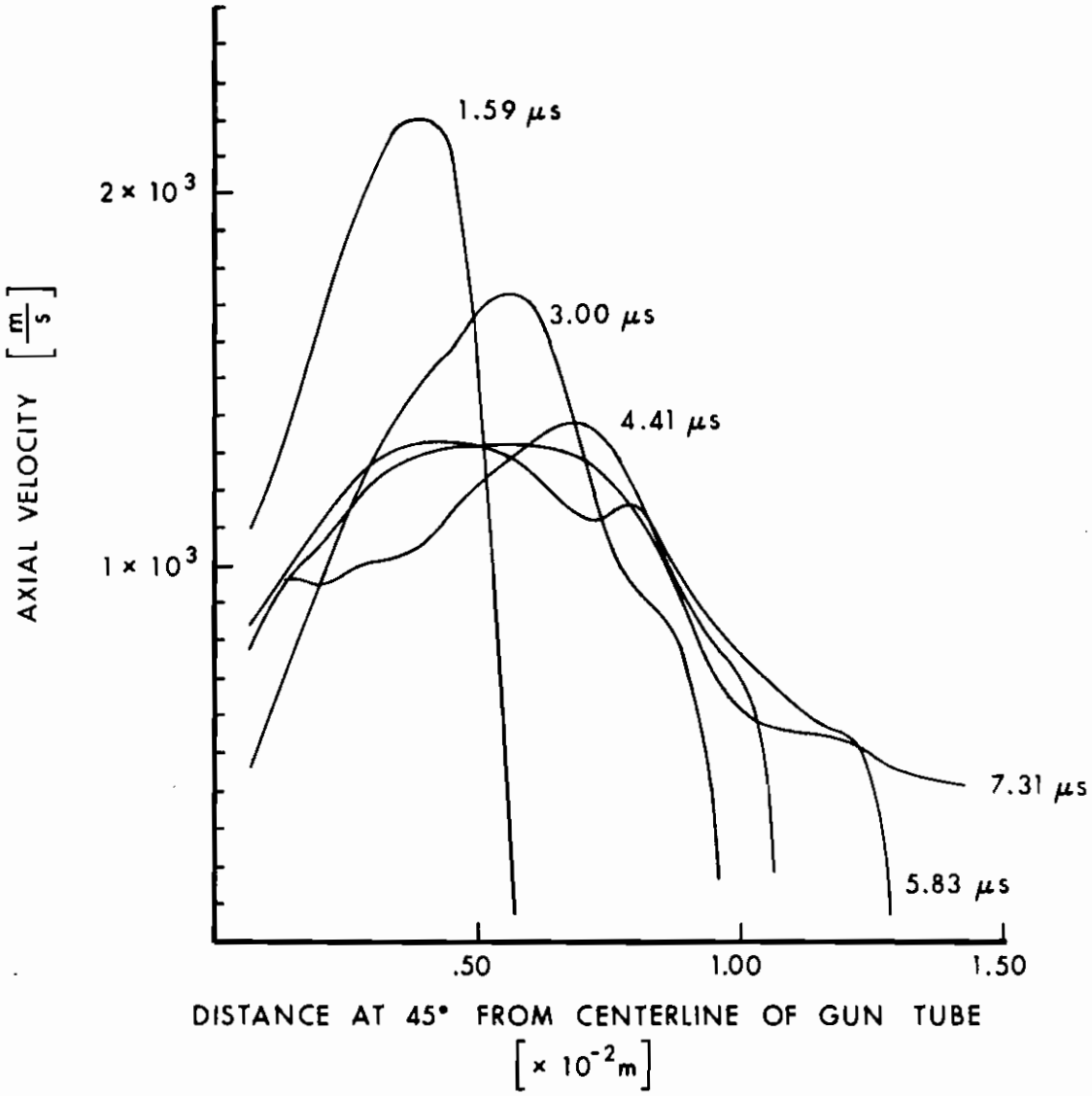
AXIAL VELOCITY [m/s]
2 × 10^3
1 × 10^3
1.59 μs
3.00 μs
4.41 μs
7.31 μs
5.83 μs
.50
1.00
1.50
DISTANCE AT 45° FROM CENTERLINE OF GUN TUBE
[× 10^-2 m]

(b)

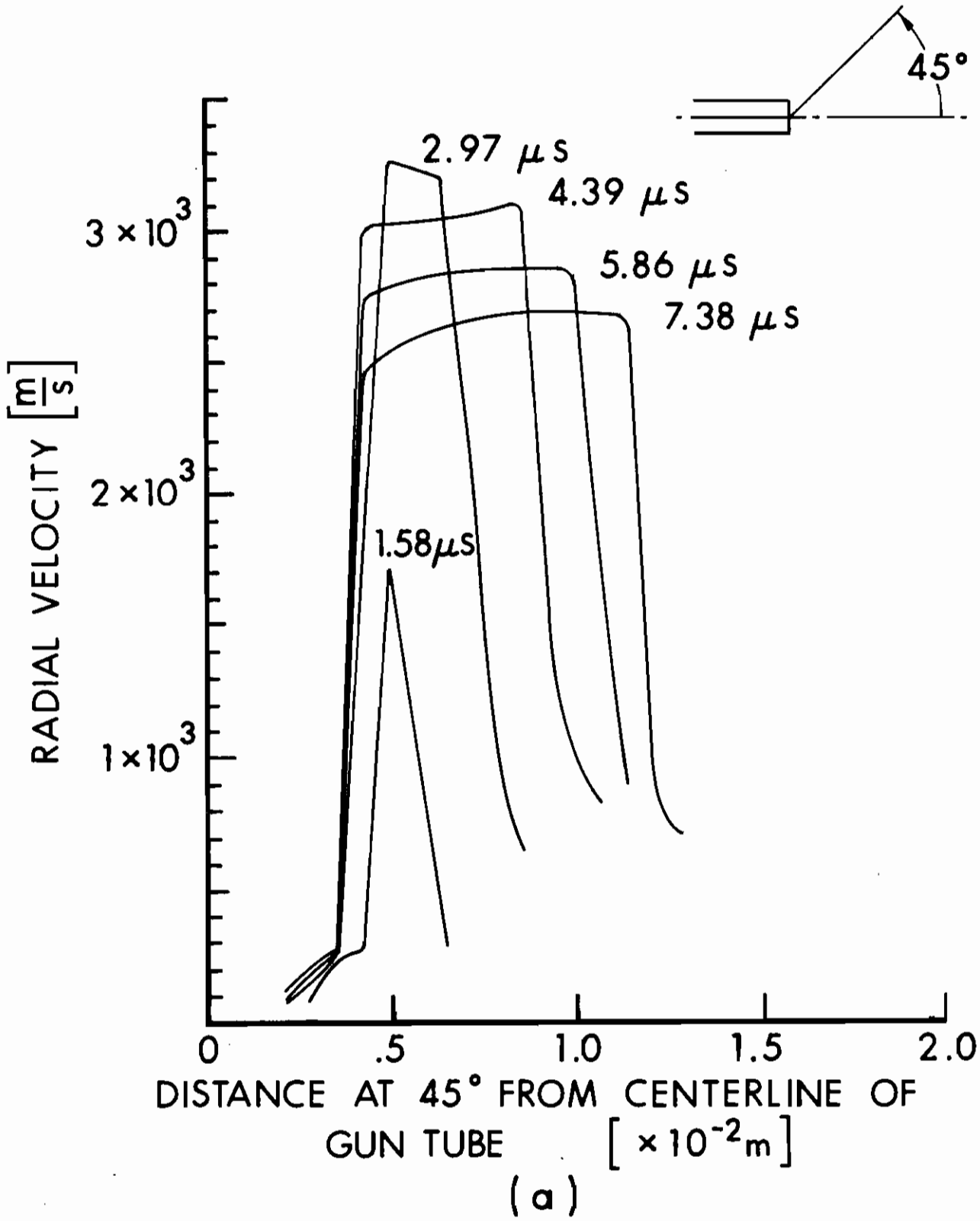

Figure 10. Radial Velocity Versus Distance at 45° from Axis of the Gun.

a. Results from the BLAST Code.
b. Results from the DORF Code.

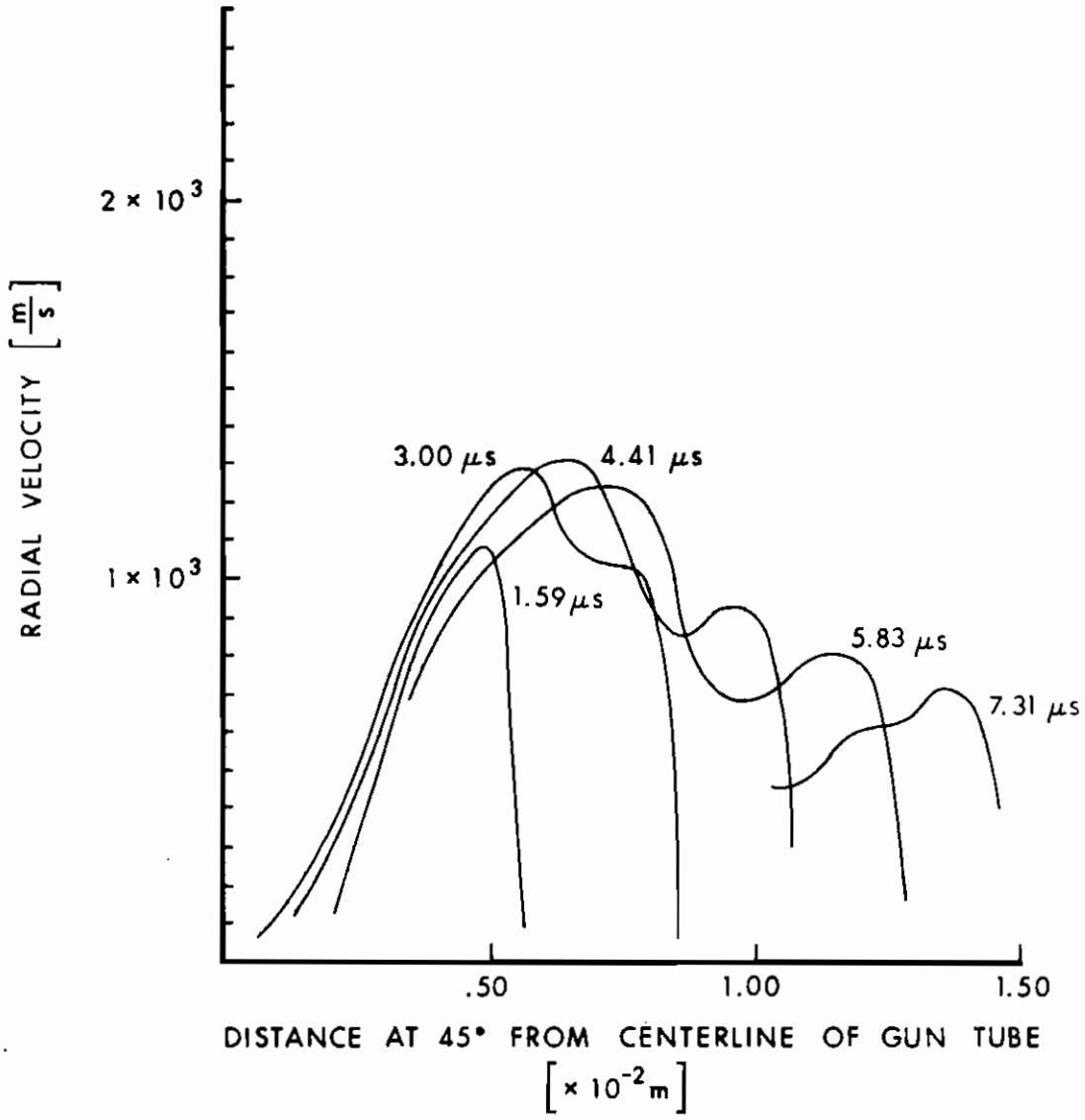
RADIAL VELOCITY $\left[\frac{m}{s}\right]$
2×10^3
1×10^3
3.00 μs
4.41 μs
1.59 μs
5.83 μs
7.31 μs
.50
1.00
1.50
DISTANCE AT 45° FROM CENTERLINE OF GUN TUBE
$\left[\times 10^{-2} m\right]$

(b)

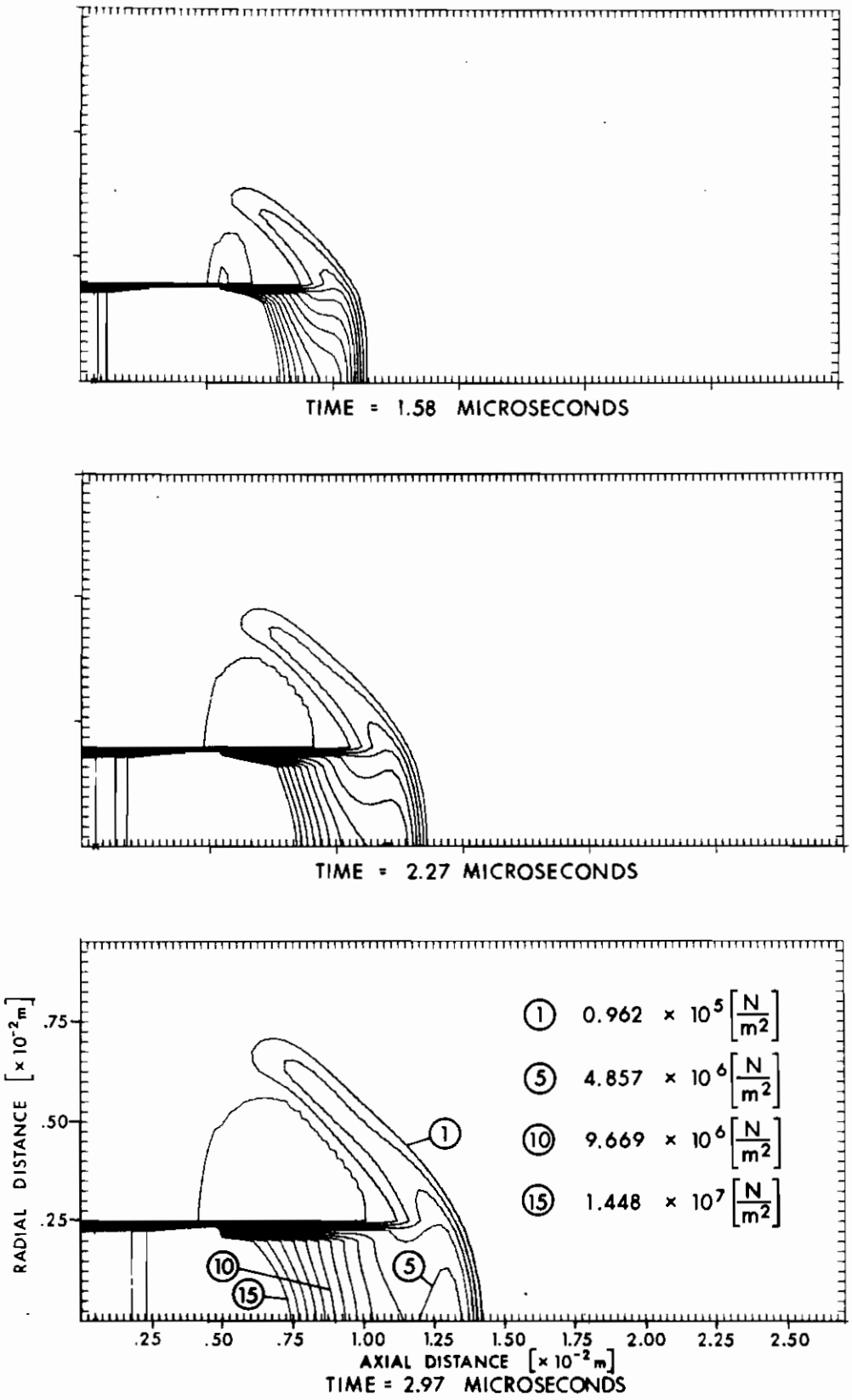

Figure 11. Pressure Contour Plots from the BLAST Code.

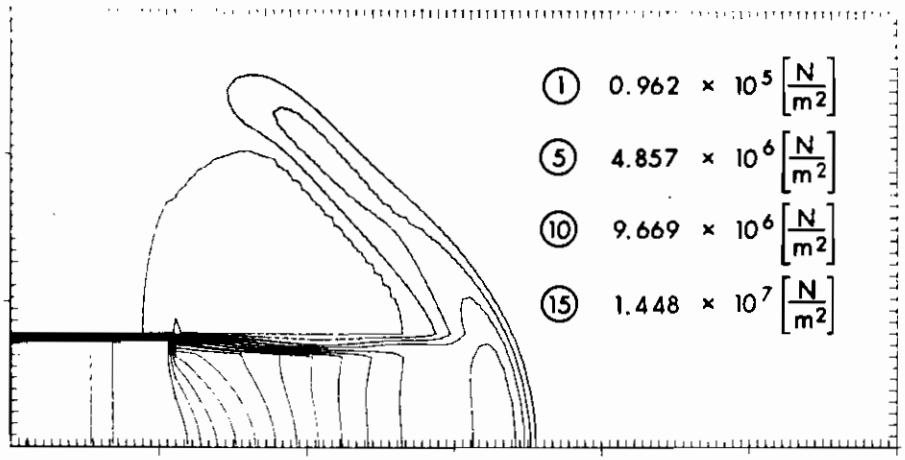

TIME = 3.68 MICROSECONDS

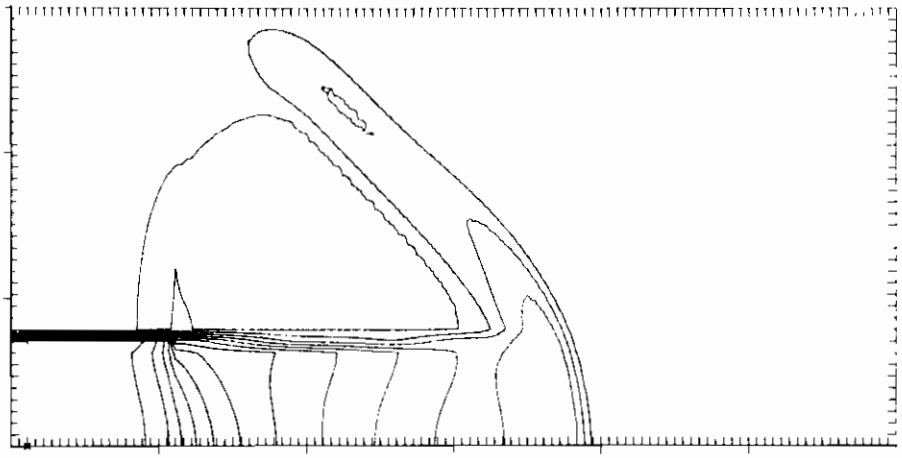

TIME = 4.39 MICROSECONDS

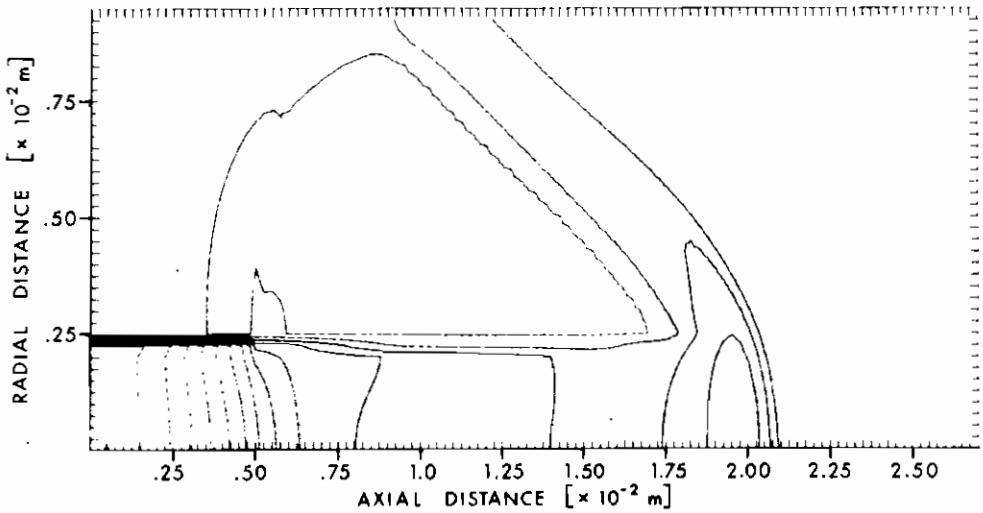

TIME = 5.86 MICROSECONDS

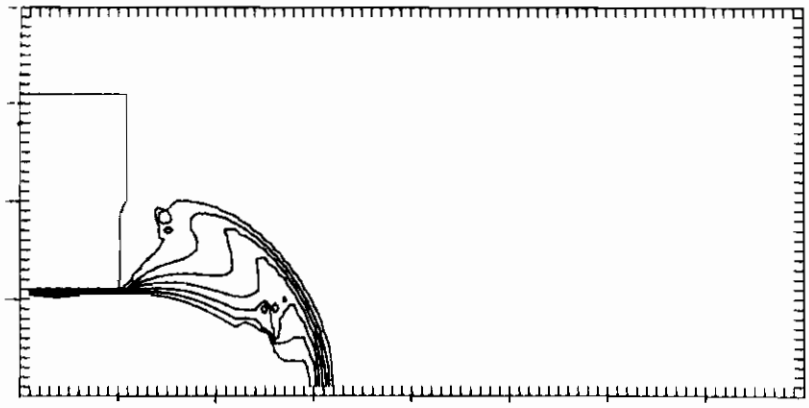

TIME = 1.59 MICROSECONDS

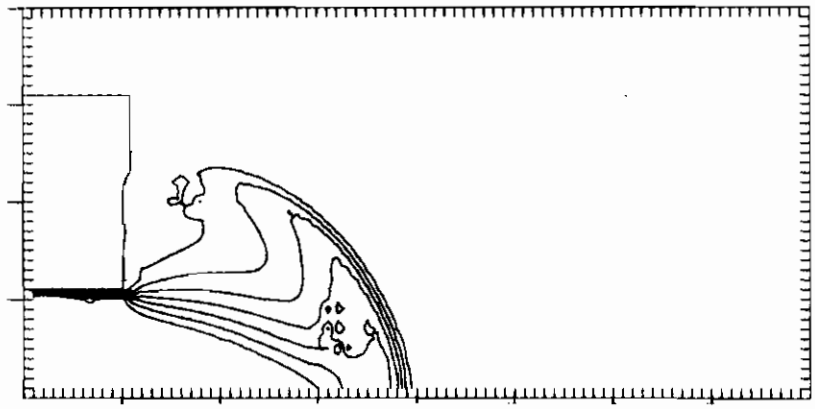

TIME = 2.26 MICROSECONDS

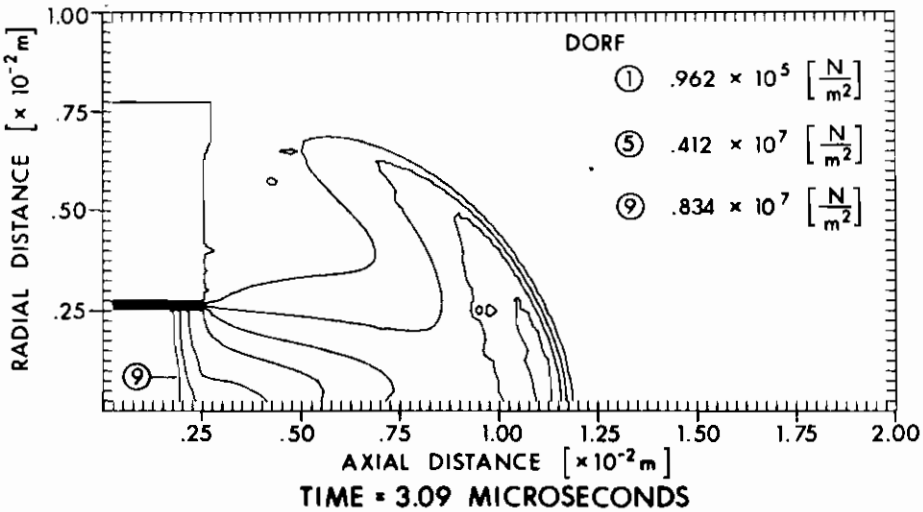

TIME = 3.09 MICROSECONDS

Figure 12. Pressure Contour Plots from the DORF Code.

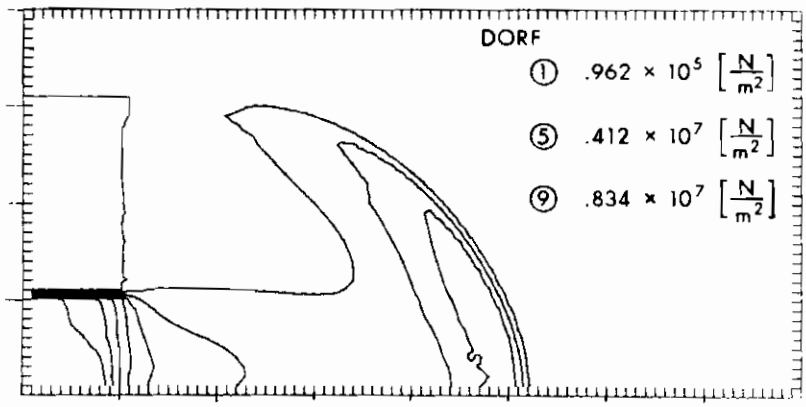

TIME = 3.63 MICROSECONDS

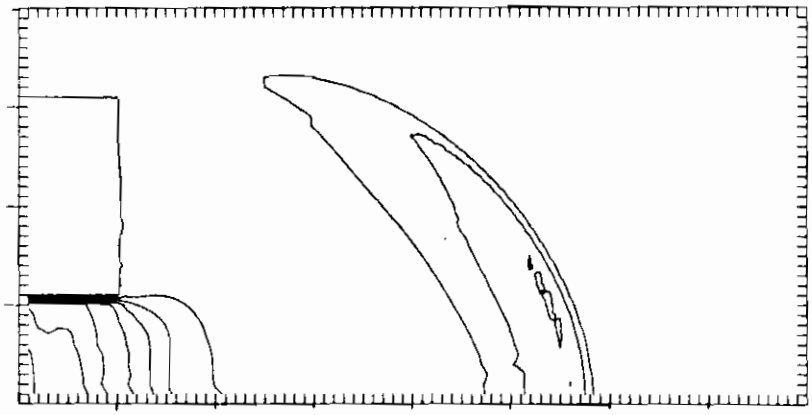

TIME = 4.41 MICROSECONDS

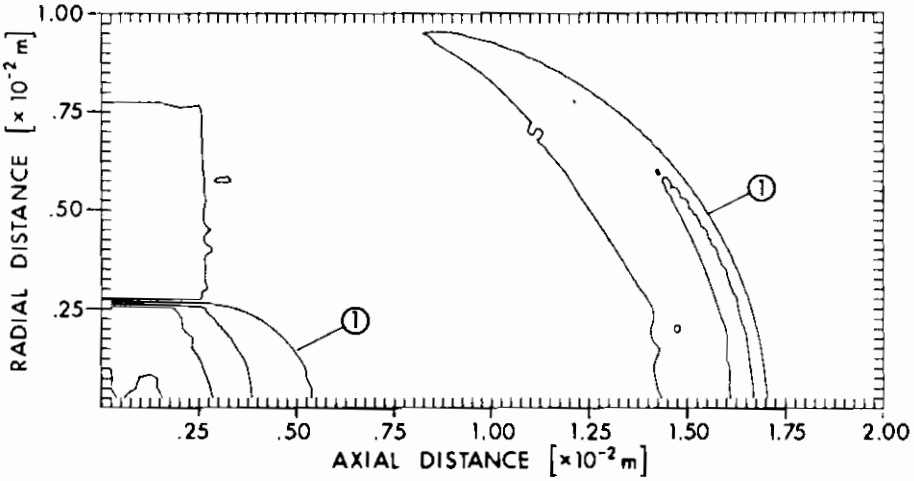

TIME = 5.83 MICROSECONDS

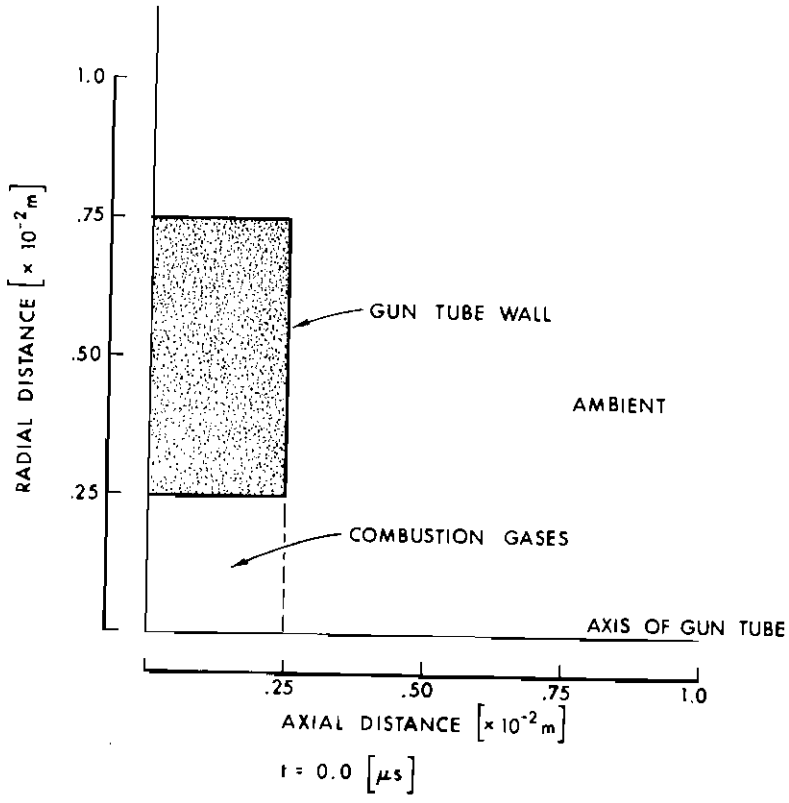

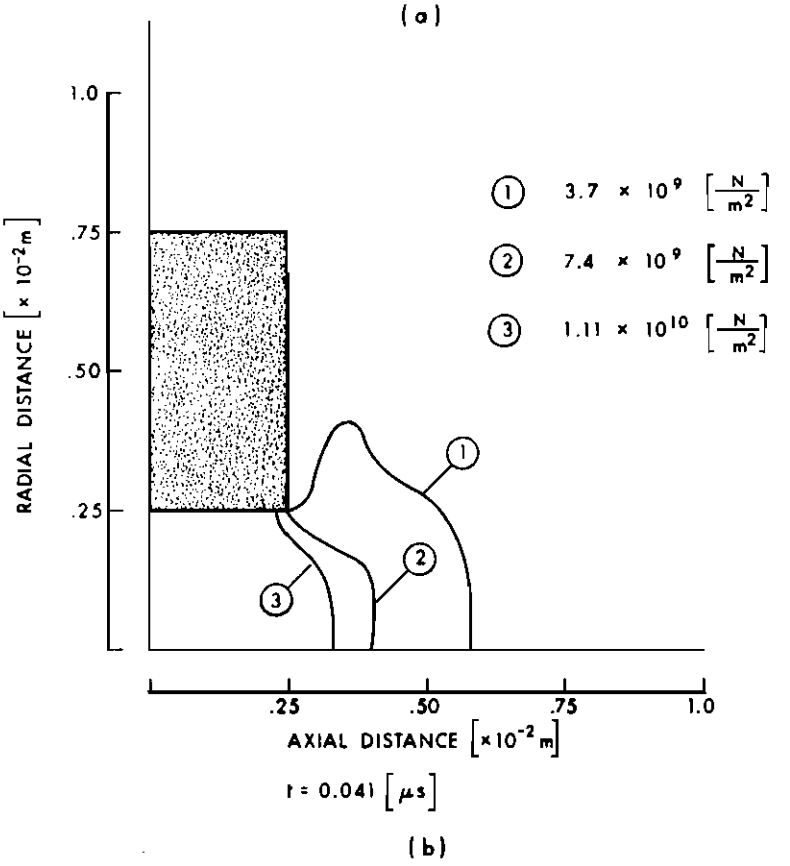

Figure 13. Flow as Calculated by the HELP Code.

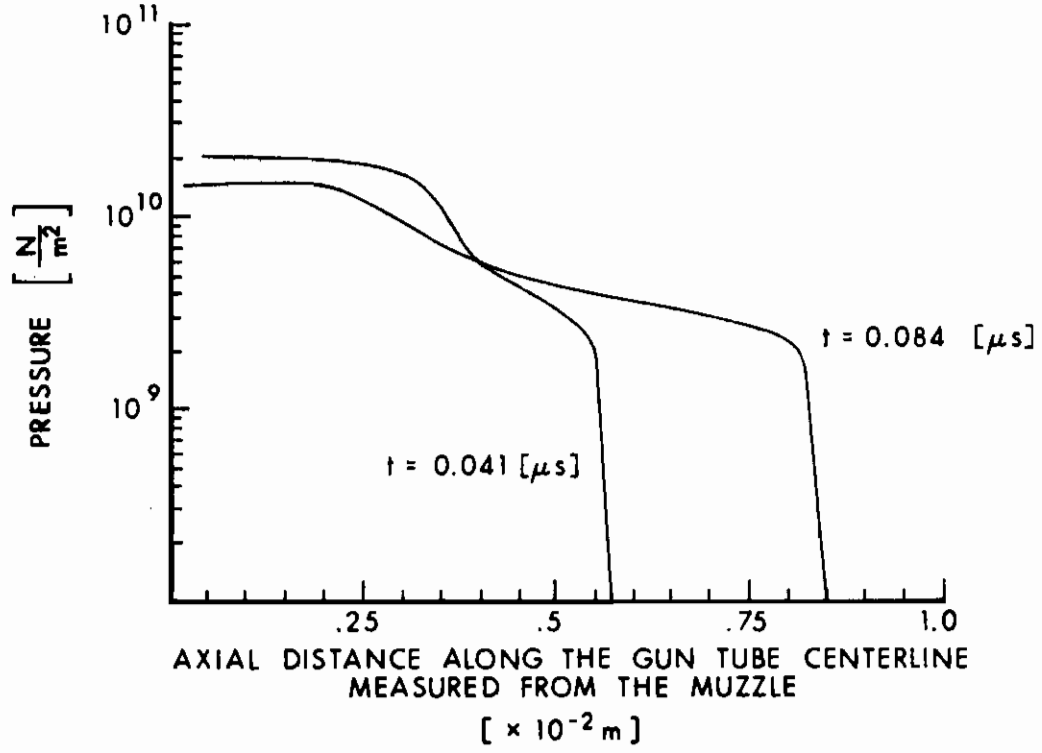

Figure 14. Pressure Versus Distance Along the Axis of the Gun Tube Calculated by HELP.

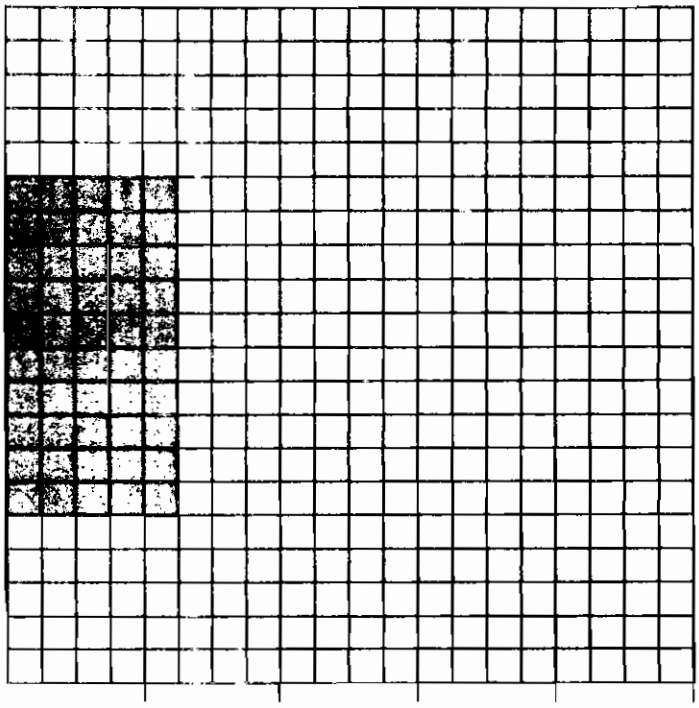

TIME = 0 01000 MICROSECONDS

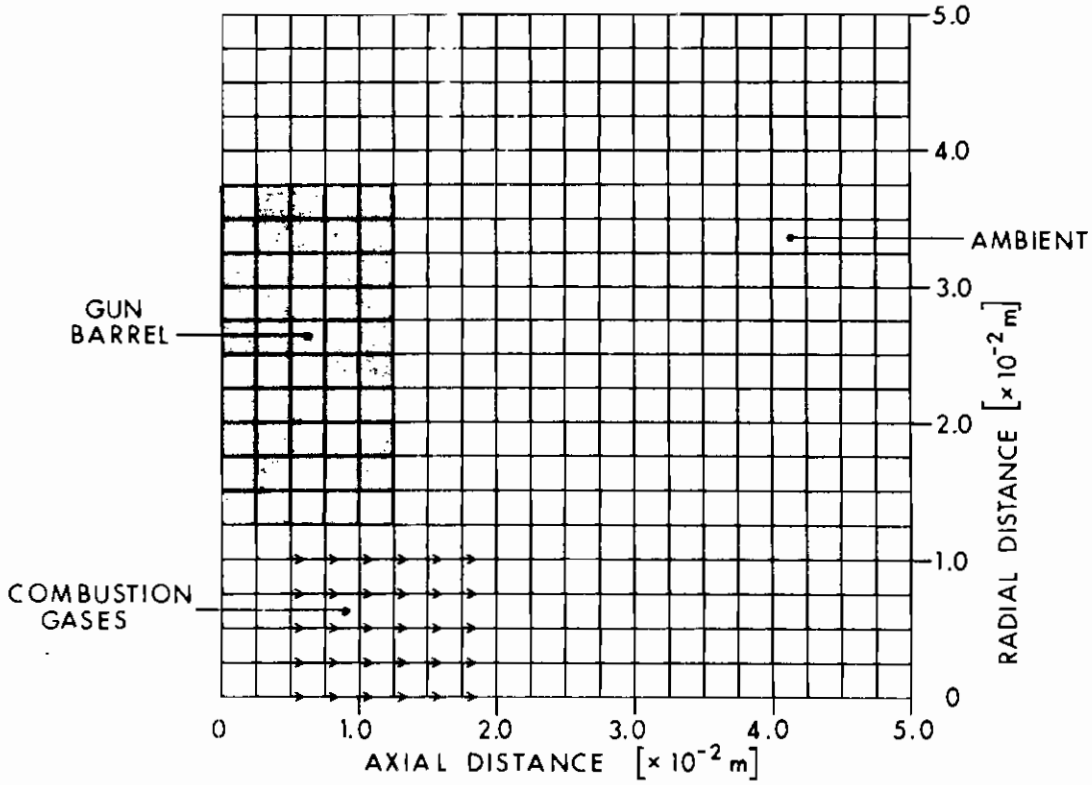

Figure 15. The Distortion of the Lagrangian Grid as Calculated by HEMP Code (6 figures).

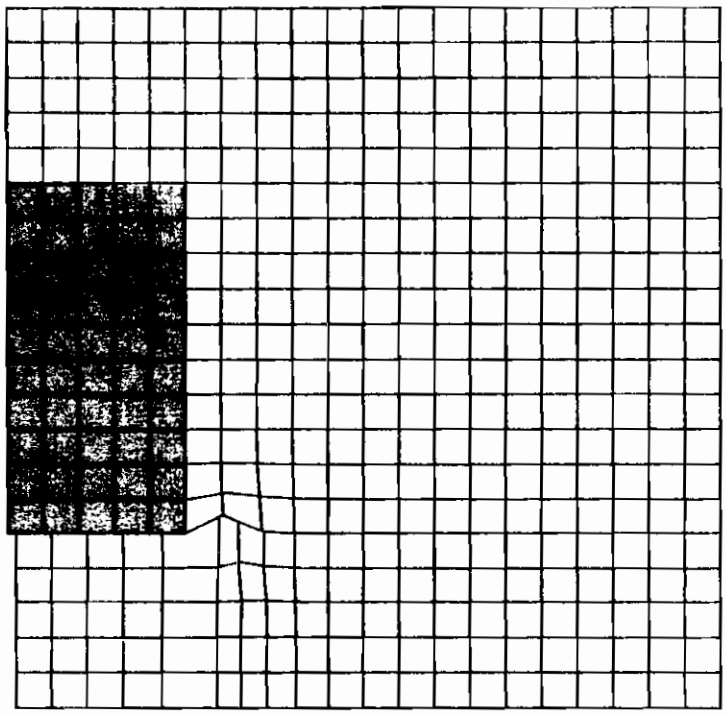

TIME = 0.10058 MICROSECONDS

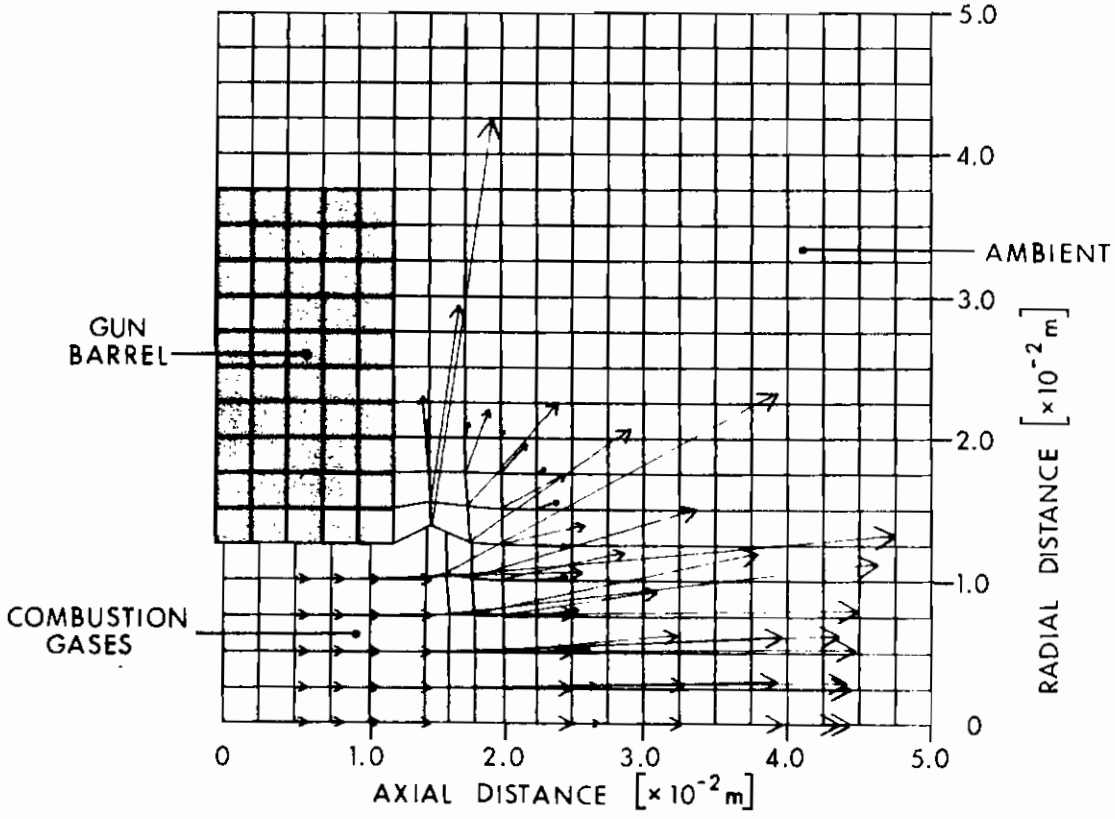

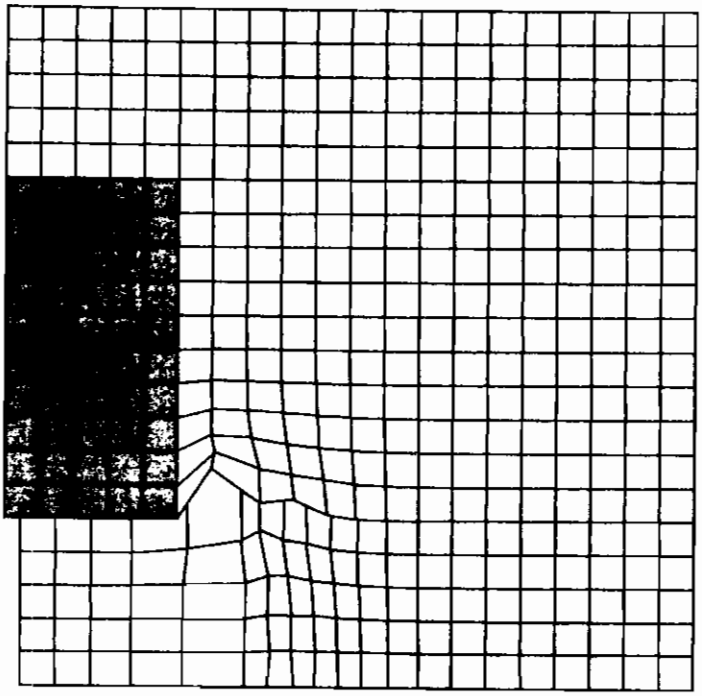

TIME = 0.20037 MICROSECONDS

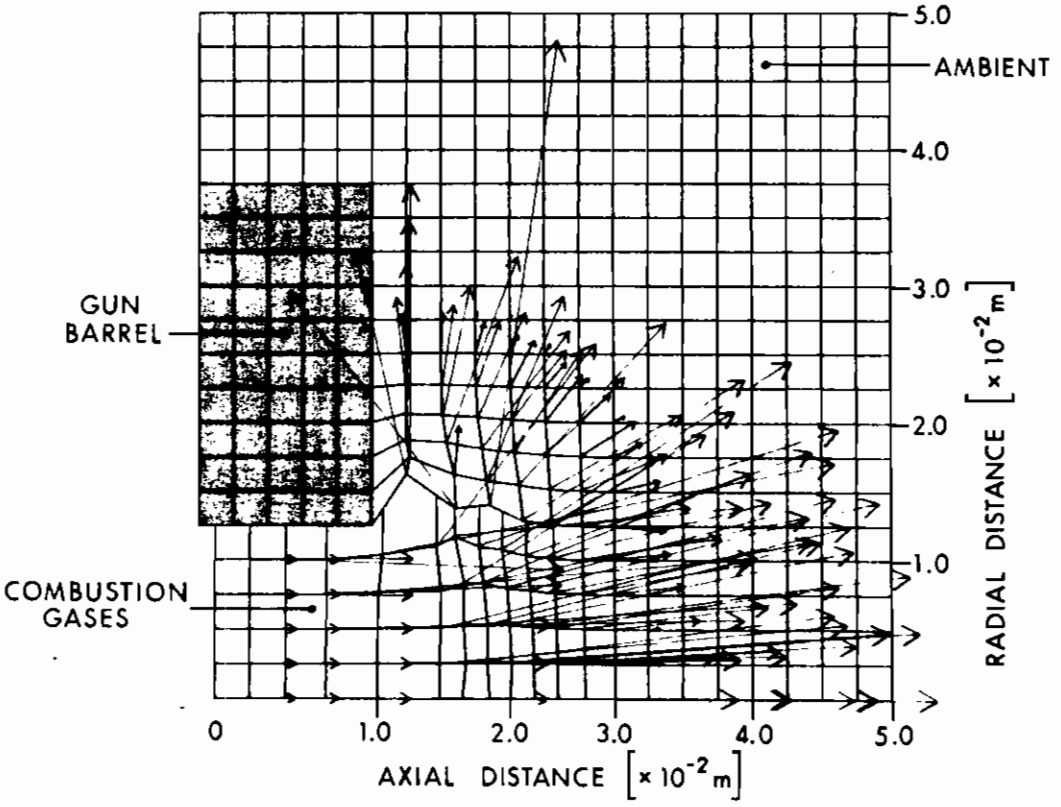

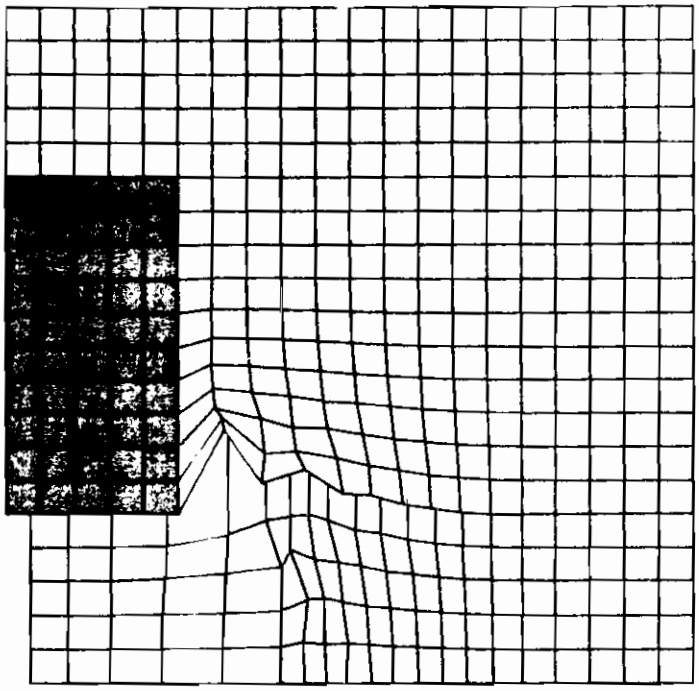

TIME = 0.30013 MICROSECONDS

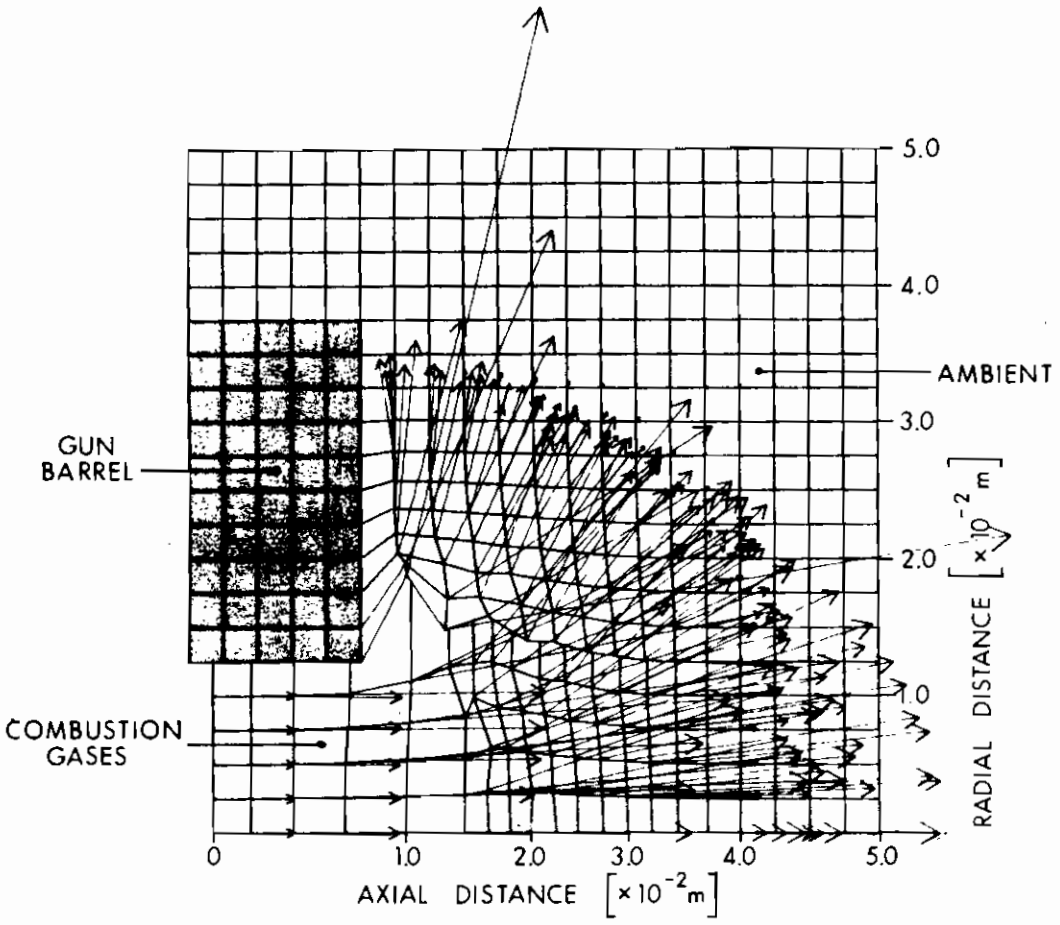

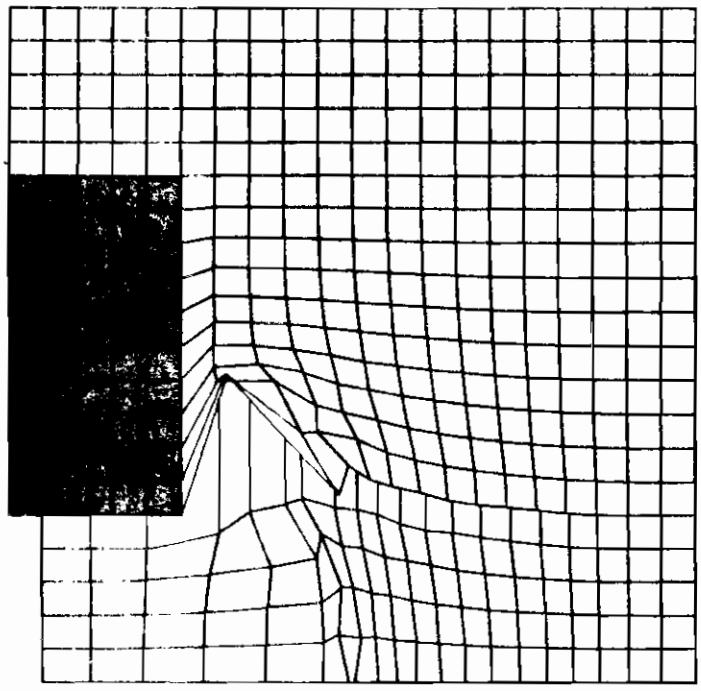

TIME = 0.39998 MICROSECONDS

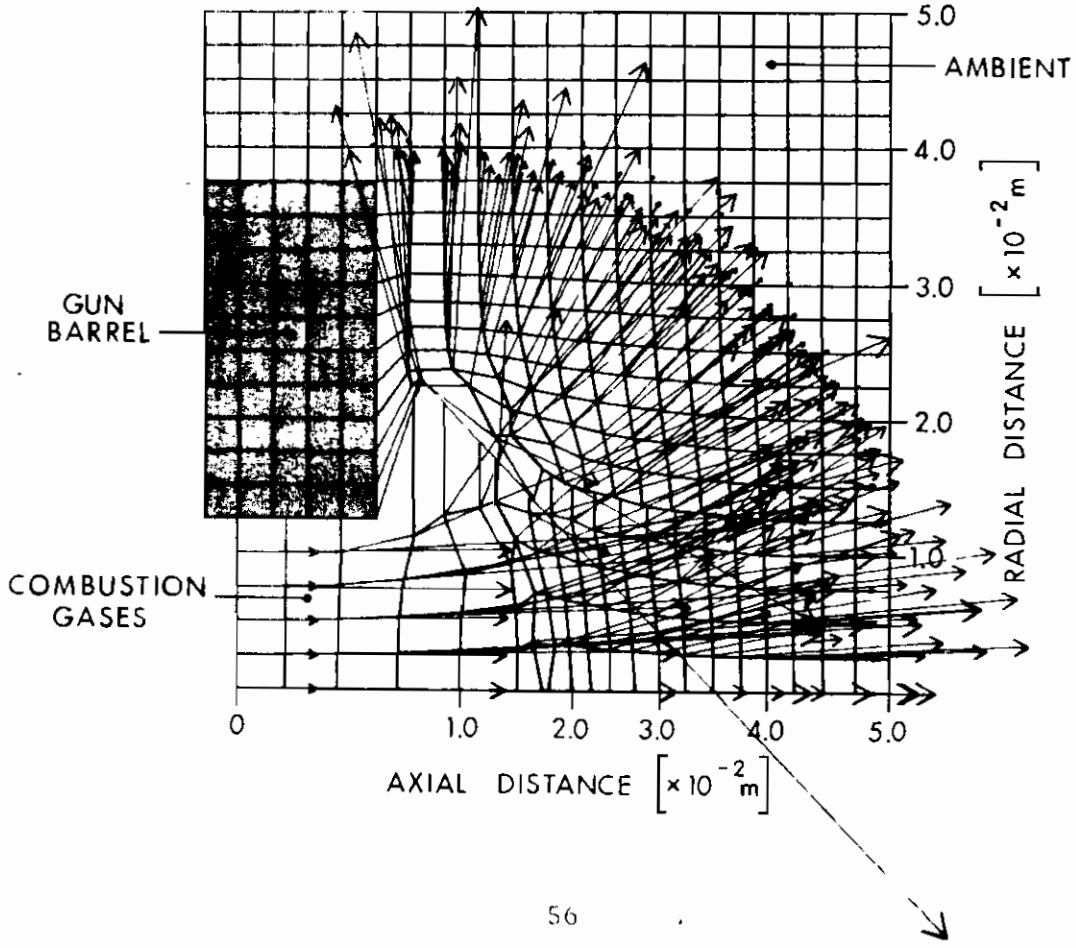

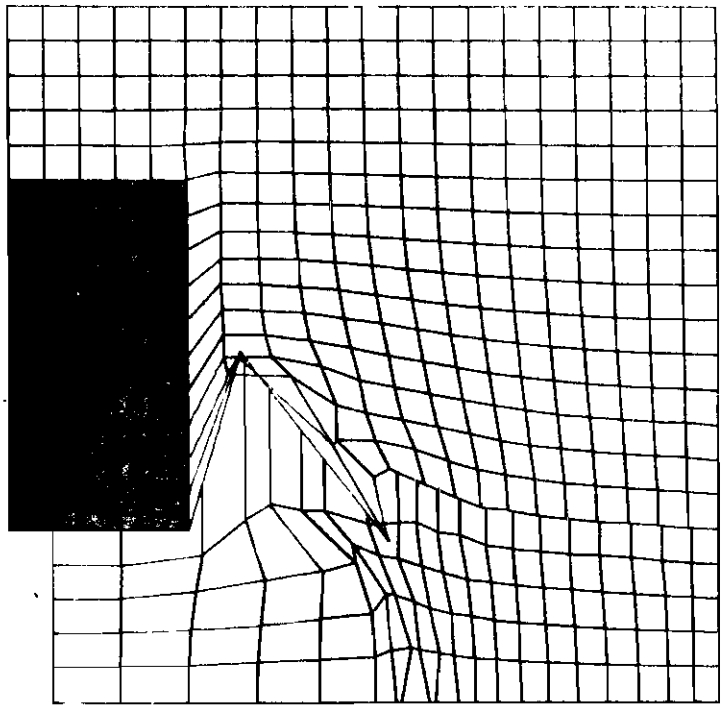

TIME = 0.50019 MICROSECONDS

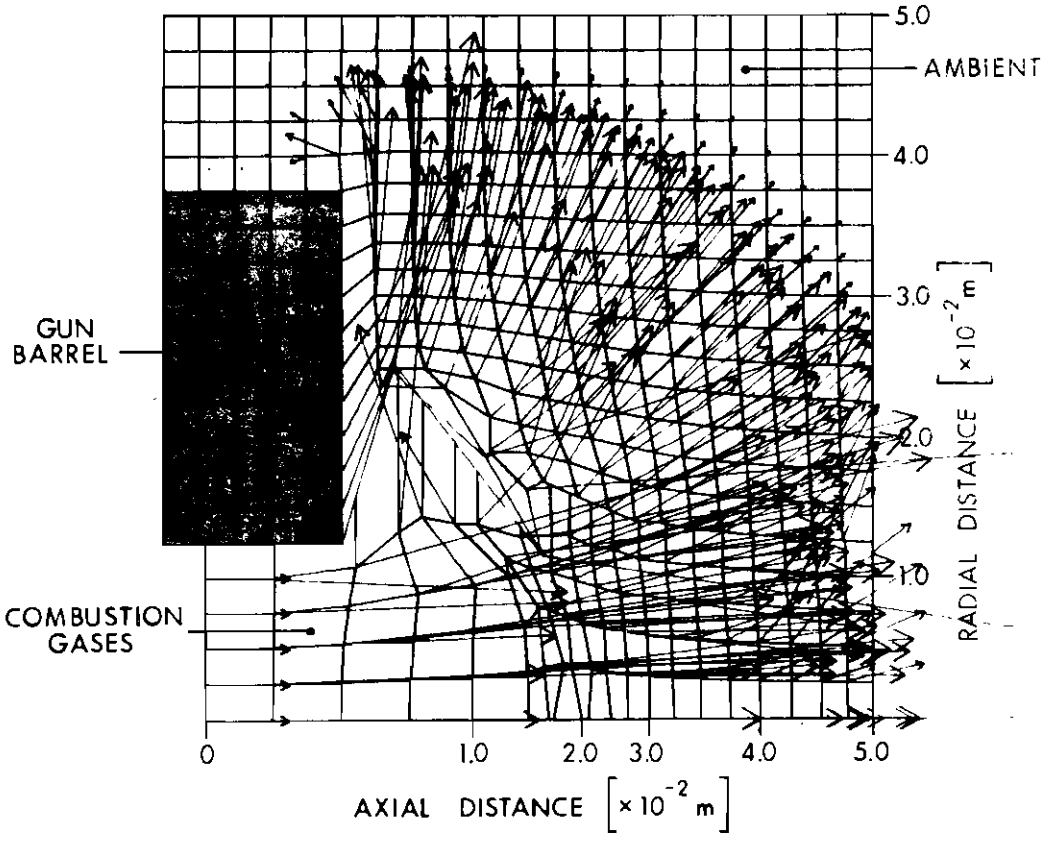

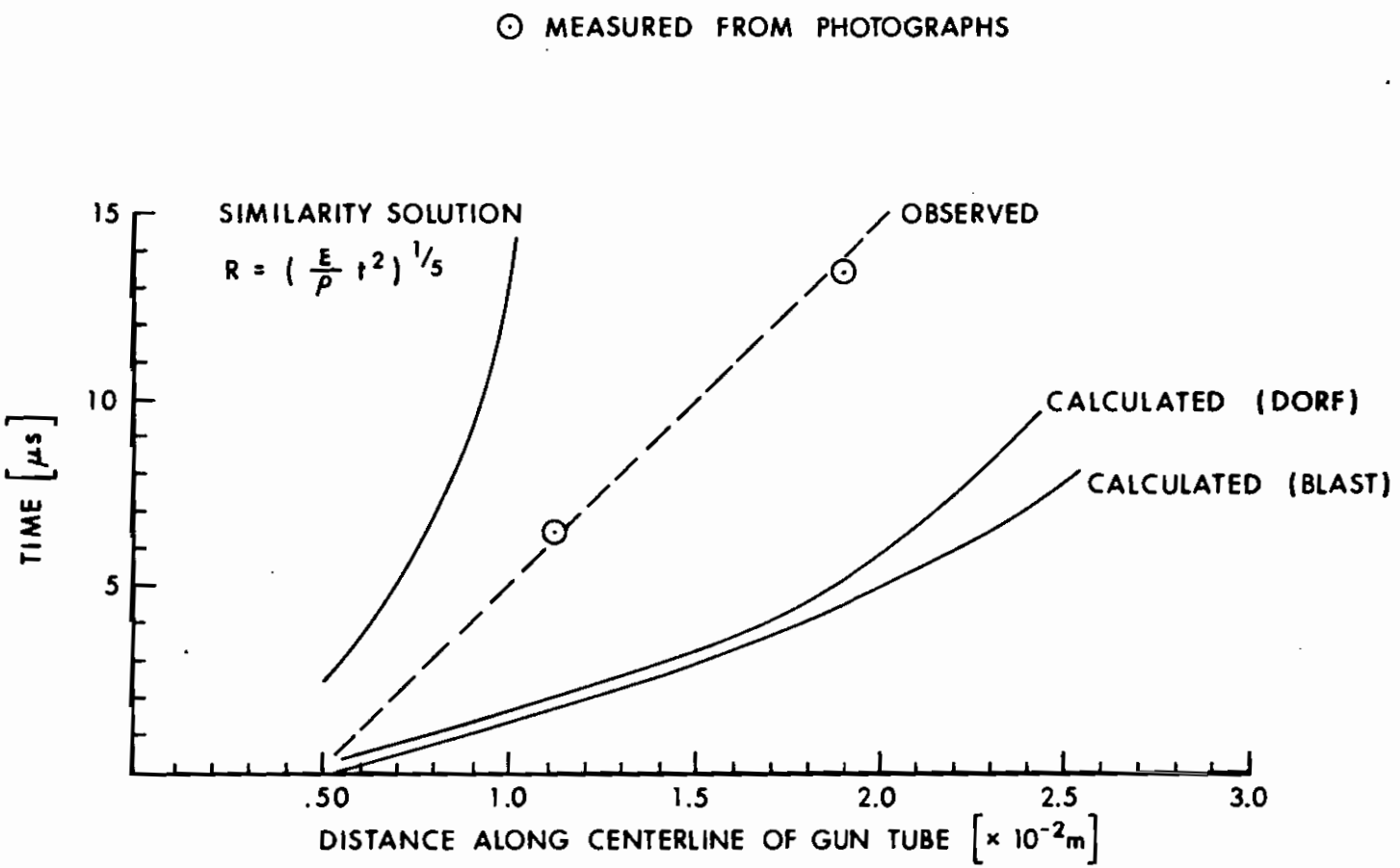

Figure 16. Comparison of Calculated and Observed Shock Location Downstream of the Muzzle as a Function of Time.

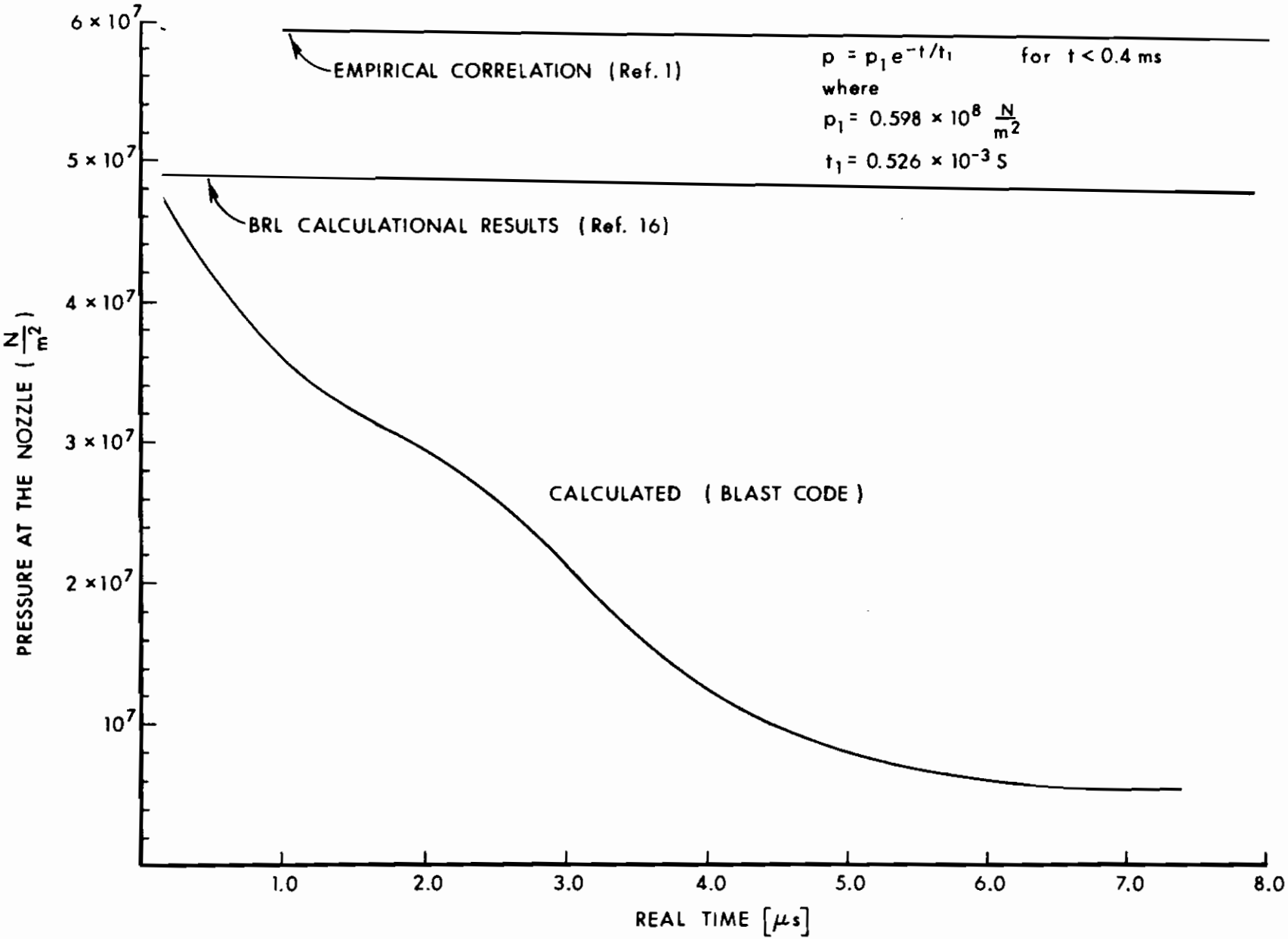

Figure 17. Comparison of an Empirical Correlation and Calculation Results of Nozzle Pressure as a Function of Time.

ACKNOWLEDGMENT

The author wishes to thank Ms. Viola Woodward, Messrs. Robert Karpp and John Harrison for their help in running the computer codes. The contour plotting routine used with the DORF code was developed by Mr. George Hartwig of AML.

REFERENCES

1. Zoltani, C.K., "Muzzle Devices, A State of the Art Survey. Vol. II: Theoretical Approaches to the Calculations of Muzzle Blast." BRL Memorandum Report No. 2294, 1973.

2. Schling, W., Sowers, D., Rogers, T., "Muzzle Brake Study for MFR Program". TRW Systems Group Report on Contract DAAF03-72-C-0018, September 15, 1972.

3. Hoo, G.S., Yagla, J. J., "Use of a Conical Muzzle Device to Control Gun Blast". NWL Technical Report TR-2793, August 1972.

4. Moore, G. R., "Finite Difference Calculations of the Free Air Gun Blast About the Muzzle of a 5/54 Naval Gun". NWL Technical Report TR-2794, September 1972.

5. Walther, M. F., "Gun Blast From Naval Guns". NWL Technical Report TR-2733, August 1972.

6. Taylor, T.D., "Calculation of Muzzle Blast Flow Fields". Technical Report 4155, Picatinny Arsenal, Dover, N.J., (1970).

7. Sinha, R., Zakkay, V., Erdos, J., "Flowfield Analysis of Plumes of Two Dimensional Underexpanded Jets by a Time Dependent Method". AIAA Journal 9, 2363-2370 (1971).

8. Private Communication form Maj. C. W. Nelson, IBL of BRL.

9. Payton, D.N., "The DORF Code User's Manual". AFWL-TR-70-60, Kirtland Air Force Base, N.M., (1970).

10. Hageman, L.J., Walsh, J. M., "HELP, A Multi-Material Eulerian Program for Compressible Fluid and Elastic-Plastic Flows in Two Space Dimensions and Time". Systems, Science, and Software Report 35R-350 (1970).

11. Wilkins, M. L., "Calculation of Elastic Plastic Flow". UCRL-7322, Rev. I, University of California, Livermore, (1969).

12. Wilkins, M.L., "Calculation of a Slender Body Moving Through Air at Supersonic and Subsonic Velocities." AIAA Journal 9, 2073-2075, (1971).

13. Brode, H.L., Enstrom, J.E., "Interior Ballistics and Gun Flash and Smoke". RAND Corp. Memorandum RM-6127-PR, October 1969.

14. Photographs, courtesy of EBL, BRL.

15. Sedov, L.I., "Similarity and Dimensional Methods in Mechanics". Academic Press, Inc., New York, 1959.

16. Crist, S., Sherman, P. M., Glas, D. R., "Study of the Highly Underexpanded Sonic Jet". AIAA Journal 4, 68-71 (1966).

17. Spong, E .D., "The Numerical Solution of the Expulsion of a Shock Wave from the Open End of a Cylindrical Shock Tube". ScD Thesis, Washington University, St. Louis, MO 1972.

18. Private Communication from Dr. A.K.R. Celmins of AML, BRL.

19. Private Communication from Mr. B.L. Morris, MERDC, Fort Belvoir, VA.

DISTRIBUTION LIST

No. of Copies	Organization
12	Commander Defense Documentation Center ATTN: TIPCR Cameron Station Alexandria, Virginia 22314
1	Director Defense Nuclear Agency Washington, DC 20305
1	Commander U.S. Army Materiel Command ATTN: AMCDL 5001 Eisenhower Avenue Alexandria, Virginia 22304
1	Commander U.S. Army Materiel Command ATTN: AMCDMA, MG J.R. Guthrie 5001 Eisenhower Avenue Alexandria, Virginia 22304
1	Commander U.S. Army Materiel Command ATTN: AMCRD, MG S. C. Meyer 5001 Eisenhower Avenue Alexandria, Virginia 22304
1	Commander U.S. Army Materiel Command ATTN: AMCRD, Dr.J.V.R.Kaufman 5001 Eisenhower Avenue Alexandria, Virginia 22304
1	Commander U.S. Army Materiel Command ATTN: AMCRD-TE 5001 Eisenhower Avenue Alexandria, Virginia 22304
1	Commander U.S. Army Materiel Command ATTN: AMCRD-TP 5001 Eisenhower Avenue Alexandria, Virginia 22304
1	Commander U.S. Army Materiel Command ATTN: AMCRD-MT 5001 Eisenhower Avenue Alexandria, Virginia 22304
1	Commander U.S. Army Materiel Command ATTN: AMCRD-W 5001 Eisenhower Avenue Alexandria, Virginia 22304
1	Commander U.S. Army Aviation Systems Command ATTN: AMSAV-E 12th and Spruce Streets St. Louis, Missouri 63166
1	Director U.S. Army Air Mobility Research and Development Laboratory Ames Research Center Moffett Field, California 94035
2	Commander U.S. Army Electronics Command ATTN: AMSEL-RD AMSEL-CE Fort Monmouth, New Jersey 07703
2	Commander U.S. Army Missile Command ATTN: AMSMI-R AMSMI-RBL Redstone Arsenal, Alabama 35809
5	Commander U.S. Army Missile Command ATTN: AMSMI-RDK Mr. R. Becht (4 cys) Mr. R. Deep Redstone Arsenal, Alabama 35809

DISTRIBUTION LIST

No. of Copies	Organization
1	Commander U.S. Army Tank Automotive Command ATTN: AMSTA-RHFL Warren, Michigan 48090
2	Commander U.S. Army Mobility Equipment Research & Development Center ATTN: Tech Docu Cen, Bldg. 315 AMSME-RZT Fort Belvoir, Virginia 22060
1	Commander U.S. Army Armament Command Rock Island, Illinois 61202
5	Commander U.S. Army Frankford Arsenal ATTN: SARFA-J8000 Mr. J. Mitchell SARFA-K3000 Mr. S. Fulton SARFA-J6300 Mr. S. Hirshman SARFA-J3000 Mr. A. Cianciosi SARFA-L4100 Mr. C. Fleischer, Jr. Philadelphia, Pennsylvania 19137
7	Commander U.S. Army Picatinny Arsenal ATTN: SARPA-AD Mr. S. Wasserman Mr. Lindner SARPA-FR Mr. A. Loeb Mr. D. Mertz Mr. E. Walbrecht Mr. S. Verner SARPA-VE, Dr. Kaufman Dover, New Jersey 07801
1	Commander U.S. Army Watervliet Arsenal Watervliet, New York 12189
1	Commander U.S. Army Safeguard Systems Command Huntsville, Alabama 35804
1	Director U.S. Army Advanced Materiel Concepts Agency 2461 Eisenhower Avenue Alexandria, Virginia 22314
1	Commander U.S. Army Harry Diamond Laboratories ATTN: AMXDO-TI Washington, DC 20438
1	Commander U.S. Army Materials and Mechanics Research Center ATTN: AMXMR-ATL Watertown, Massachusetts 02172
1	Commander U.S. Army Natick Laboratories ATTN: AMXRE, Dr. D. Sieling Natick, Massachusetts 01762
1	Deputy Assistant Secretary of the Army (R&D) ATTN: Mr. C. L. Poor Washington, DC 20310
1	Commander U.S. Army Research Officer ATTN: CRD-AA-EH Box CM, Duke Station Durham, North Carolina 27706

DISTRIBUTION LIST

No. of Copies	Organization
1	Director U.S. Army Advanced Ballistics Missile Defense Agency P. O. Box 1500 Huntsville, Alabama 35809
3	Commander U.S. Naval Air Systems Command ATTN: AIR-604 Washington, DC 20360
3	Commander U.S. Naval Ordnance Systems Command ATTN: ORD-9132 Washington, DC 20360
2	Commander and Director U.S. Naval Ship Research and Development Center ATTN: Tech Lib Aerodynamic Lab Washington, DC 20007
3	Commander U.S. Naval Weapons Center ATTN: Code 753, Tech Lib Code 50704, Dr. W. Haseltine Code 3007, Mr. A. Rice China Lake, California 93555
4	Commander U.S. Naval Ordnance Laboratory ATTN: Code 031, Dr. K. Lobb Code 312, Mr. R. Regan Mr. S. Hastings Code 730, Tech Lib Silver Spring, Maryland 20910
3	Director U.S. Naval Research Laboratory ATTN: Tech Info Div Code 7700, Dr. A. Kolb Code 7720, Dr. E. McClean Washington, DC 20390
1	Commander U.S. Naval Weapons Laboratory ATTN: Code GX, Dr. W. Kemper Dahlgren, Virginia 22448
2	Commander U.S. Naval Ordnance Station Indian Head, Maryland 20640
2	ADTC (ADBPS-12) Eglin AFB Florida 32542
1	AFATL (DLR) Eglin AFB Florida 32542
1	AFATL (DLRD) Eglin AFB Florida 32542
1	AFATL (DLRV) Eglin AFB Florida 32542
2	AFATL (DLRA, Mr. F. Burgess; Tech Lib) Eglin AFB Florida 32542
1	AFWL (DEV) (WLIL) Kirtland AFB New Mexico 87117
1	ARD (ARIL) Wright-Patterson AFB Ohio 45433
1	ARL Wright-Patterson AFB Ohio 45433
1	ASD (ASBEE) Wright-Patterson AFB Ohio 45433

DISTRIBUTION LIST

No. of Copies	Organization
1	RTD (RDFE, Mr. Sedderke) Wright-Patterson AFB Ohio 45433
1	Director National Bureau of Standards ATTN: Tech Lib U.S. Department of Commerce Washington, DC 20234
1	Headquarters National Aeronautics and Space Administration ATTN: Code EP, M. Adams Washington, DC 20546
1	Director NASA Scientific and Technical Information Facility ATTN: SAK/DL P. O. Box 33 College Park, Maryland 20740
1	Director Jet Propulsion Laboratory ATTN: Tech Lib 4800 Oak Grove Drive Pasadena, California 91103
2	Director National Aeronautics and Space Administration George C. Marshall Space Flight Center ATTN: MS-I, Lib R-AERO-AE, Mr. A. Felix Huntsville, Alabama 35812
1	Director National Aeronautics and Space Administration Langley Research Center ATTN: MS 185, Tech Lib Langley Station Hampton, Virginia 23365
1	Director National Aeronautics and Space Administration Lewis Research Center ATTN: MS 60-3, Tech Lib 21000 Brookpark Road Cleveland, Ohio 44135
1	Advanced Technology Laboratory ATTN: Dr. J. Erdos 400 Jericho Turnpike Jericho, New York 11753
2	ARO, Inc. ATTN: Tech Lib Arnold AFS Tennessee 37389
1	Technical Director Colt Firearms Corporation 150 Hyshore Avenue Hartford, Connecticut 14061
1	General Electric Corporation Armaments Division ATTN: Mr. R. Whyte Lakeside Avenue Burlington, Vermont 05401
1	Winchester-Western Division Olin Corporation ATTN: Mr. D. Mettill New Haven, Connecticut 06504
1	Sandia Corporation ATTN: Aerodynamics Dept Org 5620, Mr. R. Maydew P. O. Box 5800 Albuquerque, New Mexico 87115
1	California Institute of Technology Aeronautics Department ATTN: Prof. H. Liepmann Pasadena, California 91102

DISTRIBUTION LIST

No. of Copies	Organization
1	Guggenheim Aeronautical Laboratory California Institute of Technology ATTN: Tech Lib Pasadena, California 91104
3	Calspan Corporation ATTN: Mr. J. Martin Dr. W. Wurster Dr. G. Skinner P. O. Box 235 Buffalo, New York 14221
2	Franklin Institute ATTN: Dr. Carfagno Dr. Wachtell Race & 20th Streets Philadelphia, Pennsylvania 19103
1	Director Applied Physics Laboratory The Johns Hopkins University 8621 Georgia Avenue Silver Spring, Maryland 20910
1	Massachusetts Institute of Technology Department of Aeronautics and Astronautics ATTN: Tech Lib 77 Massachusetts Avenue Cambridge, Massachusetts 02139
1	Director Guggenheim Aerospace Labs New York University New York Heights New York, New York 10053
1	Ohio State University Department of Aeronautics and Astronautical Engineering ATTN: Tech Lib Columbus, Ohio 43210
1	Polytechnic Institute of Brooklyn Graduate Center ATTN: Dr. G. Morretti Farmingdale, New York 11735
1	Director Forrestal Research Center Princeton University Princeton, New Jersey 08540
1	Princeton University Forrestal Laboratories ATTN: Dr. S. I. Cheng Princeton, New Jersey 08540
2	University of Mechigan Department of Aeronautical Engineering ATTN: Dr. A. Kuethe Dr. M. Sichel East Engineering Building Ann Arbor, Michigan 48104
	Aberdeen Proving Ground
	Ch, Tech Lib Marine Corps Ln Ofc Cmdr, USALWL Cmdr, USATECOM ATTN: AMSTE-BE, Mr. Morrow AMSTE-TA-R, Mr. Wise Dir, USAMSAA

INTENTIONALLY LEFT BLANK.

DOCUMENT CONTROL DATA - R & D

(Security classification of title, body of abstract and indexing annotation must be entered when the overall report is classified)

1. ORIGINATING ACTIVITY *(Corporate author)*
USA Ballistic Research Laboratories
Aberdeen Proving Ground, Maryland 21005

2a. REPORT SECURITY CLASSIFICATION
Unclassified

2b. GROUP
N/A

3. REPORT TITLE
Evaluation of the Computer Codes BLAST, DORF, HELP and HEMP for Suitability of Underexpanded Jet Flow Calculation.

4. DESCRIPTIVE NOTES *(Type of report and inclusive dates)*

5. AUTHOR(S) *(First name, middle initial, last name)*
Csaba K. Zoltani

6. REPORT DATE	7a. TOTAL NO. OF PAGES	7b. NO. OF REFS
AUGUST 1973	67	19

8a. CONTRACT OR GRANT NO.	9a. ORIGINATOR'S REPORT NUMBER(S)
b. PROJECT NO. 1J562604A607	BRL REPORT NO. 1659
c.	9b. OTHER REPORT NO(S) *(Any other numbers that may be assigned this report)*
d.	

10. DISTRIBUTION STATEMENT
Approved for public release; distribution unlimited.

11. SUPPLEMENTARY NOTES	12. SPONSORING MILITARY ACTIVITY
	US Army Materiel Command 5001 Eisenhower Avenue Alexandria, Virginia 22304

13. ABSTRACT

The computer codes BLAST, DORF, HELP and HEMP have been used to simulate the flow field at the muzzle of a M-16 rifle, without any deflectors, compensators, or flash hiders. The flow was modeled as an underexpanded jet, of a compressible, inviscid and non-reactive gas. The calculations, restricted to the initial stages of formation of the jet were done on a cylindrically symmetric geometry without the presence of a flow obstruction in the form of a projectile. Results are presented as pressure contours as well as pressure and velocity profiles at different angles from the centerline of the muzzle of the barrel, and plots of pressure versus distance from the muzzle. The calculations are compared with available photographic records of the process.

14 KEY WORDS	LINK A		LINK B		LINK C	
	ROLE	WT	ROLE	WT	ROLE	WT
Muzzle Blast						
Gas Dynamics						
Shock Waves						
Numerical Analysis						
Computer Codes						